Grid connected Active Front End rectifier fed Dual Active Bridge for EV battery Charging

A PROJECT REPORT

SUBMITTED IN PARTIAL FULFILLMENT OF THE REQUIREMENTS
FOR THE AWARD OF THE DEGREE
OF

MASTER OF TECHNOLOGY

IN

POWER ELECTRONICS AND SYSTEMS

Submitted by

Ashish Mishra

(2K21/PES/05)

Under the supervision of

Prof. Mukhtiar Singh

DEPARTMENT OF ELECTRICAL ENGINEERING

DELHI TECHNOLOGICAL UNIVERSITY

(Formerly Delhi College of Engineering) Bawana Road, Delhi-110042

May 2023

DEPARTMENT OF ELECTRICAL ENGINEERING
DELHI TECHNOLOGICAL UNIVERSITY
(Formerly Delhi College of Engineering)Bawana Road, Delhi-110042

CANDIDATE'S DECLARATION

I attest that the following is true:

a. The work in this report is original and was completed by me with the help of my supervisor.

a. When drafting the report, I adhered to the instructions given by the Institute.

c. I abide by the standards and principles outlined in the Institute's Ethical Code of Conduct.

d. I always gave credit where credit is due when using resources (data, theoretical analysis, figures, and text) from other sources by citing them in the report's text and providing further information in the references.

Additionally, I have always sought permission from the materials' copyright holders.

Place: Delhi

Ashish Mishra
(2K21/PES/05)

Date: 31.05.2023

DEPARTMENT OF ELECTRICAL ENGINEERING

DELHI TECHNOLOGICAL UNIVERSITY

(Formerly Delhi College of Engineering)Bawana Road, Delhi-110042

CERTIFICATE

I certify that the Project Dissertation titled "Grid connected Active Front End rectifier fed Dual Active Bridge for EV battery Charging" was submitted by Ashish Mishra, Roll No – 2K21/PES/05. here, Electrical Engineering, Delhi Technological University, Delhi in partial fulfilment of the requirement for the award of the degree of Master of Technology, is a recordof the project work carried out by the students under my supervision. To the best of my knowledge, this work has not been submitted in part or full for any Degree or Diploma to this University or elsewhere.

SUPERVISOR

Place: Delhi

Prof. Mukhtiar Singh

Date: 31.05.2023

ABSTRACT

Electric vehicles (EVs), which are gaining popularity as a green and effective method of transportation, have significantly accelerated the electrification of transportation in recent years. The effective charging of the electric vehicle battery is one of the main issues facing EV adoption. AC/DC and DC/DC converter-based charging systems have become crucial parts of the EV charging infrastructure as a solution to this problem. In order to minimize charging time, increase charging efficiency, and guarantee the longevity of the EV battery, efficient power conversion in both the AC/DC and DC/DC converters is essential. Therefore, to improve the effectiveness and performance of these converters, cutting-edge power electronics technologies are being used, such as wide-bandgap semiconductors (such as silicon carbide and gallium nitride) and high-frequency switching techniques.

This thesis describes the implementation of a three-phase grid-connected electric vehicle (EV) battery charging system made up of two conversion stages: an AC-DC stage with a three-phase Active Front End (AFE) rectifier and a DC-DC stage with a single-phase Dual Active Bridge (DAB) converter. Because of its high voltage conversion ratio, power density, and galvanic isolation, the DAB is chosen for the DC-DC stage. The AC-DC stage's LCL filter at the input is made to suppress the harmonics in the input current. To obtain the necessary DC link voltage, the active front-end rectifier is under decoupled DQ control. To increase battery voltage and decrease ripples, the Dual Active Bridge (DAB) is controlled in a closed loop using an LC output filter. For various load values, all of the switches achieve zero voltage switching (ZVS), which enables the converter to have reduced switching loss and provides higher efficiency. The system is designed for a 10-kW power rating, and MATLAB/Simulink is used to simulate the system under various load circumstances in order to assess the resilience of the converter and controller.

.

DEPARTMENT OF ELECTRICAL ENGINEERING
DELHI TECHNOLOGICAL UNIVERSITY
(Formerly Delhi College of Engineering)Bawana Road, Delhi-110042

ACKNOWLEDGEMENT

First and foremost, I want to give praise and thanks to GOD (the Cherisher of the Whole Universe), who gave me enough direction and kindness to complete this work.

It gives me great pleasure to take use of this chance to work under the gracious supervision of Prof. Mukhtiar Singh at the DTU (Department of Electrical Engineering) in Delhi.

First and foremost, I would like to express my sincere gratitude, appreciation, and debt of gratitude to Prof. Mukhtiar Singh for his excellent advice, ongoing support, profound inspiration, and ready assistance during the project work.

I owe a debt of gratitude to my parents, Mrs. Surabhi Mishra & Mr. Ram Naresh Mishra, for their invaluable counsel, loving inspiration, and encouragement at every level of my academic career.

Last but not least, I want to express my sincere gratitude to my friends for helping me with the preparation of this project report.

Place: Delhi

Ashish Mishra

(2K21/PES/05)

Date: 31.05.2023

CONTENTS

LIST OF TABLES

LIST OF FIGURES

CHAPTER-1
INTRODUCTION

1.1 BACKGROUND

In response to developing worries about climate change, several governmental and business stakeholders have advocated reduction in utilizing petroleum as the direct energy source to power transport system. When battery electric cars (EVs) are connected to the grid, the on-board battery systems can be recharged with environmentally friendly, natural energy sources, which can help cut down on the consumption of petroleum.

When converting to an electrically powered transport system, a battery backup that can support the vehicle's energy and power requirements is required. The practicality and affordability of EVs have grown as a result of the significant breakthroughs made in lithium-ion batteries over the past several years. The cost of batteries has significantly decreased and is currently approximately $120 per kWh. [1]– [3]. In spite of enormous enhancement in Li-ion battery energy density and higher efficiency, the range of driving electric vehicles for a single charge is still less as compared to traditional petrol vehicles owing to the orders of magnitude greater energy density compared to petroleum. In conclusion, there are still considerable obstacles preventing a more general adoption of EVs, including lithium-ion battery deterioration at relaxation and during periods, electrochemical process constraints on charging rate, and low energy density (in comparison to petroleum). Even if costs are going down and performance has considerably increased, this is still the case.

Along with the drawbacks of Li-ion battery technology, the lack of a refilling structure can rapidly and smoothly recharge Electric Vehicle to increase driving on long excursions continues to be a key barrier to the widespread adoption of EVs. Consequently, there is an immediate need for a parallel EV charging infrastructure to complement existing diesel fuel stations, particularly in areas where long travelling is prevalent. When creating and implementing such an infrastructure for charging electric vehicles, a complex range of technical and policy implications, taking into account conflicting industry norms, accessible advances in technology, grid effects, and other technological difficulties.

Modern dc fast chargers employ two power conversion stages to transform 3-phase input ac voltage up to 480 V into the required V_{DC}: an AC-DC stage with PFC, which transforms 3-phase ac voltage into the desired V_{DC}; and a DC-DC stage, which transforms the output dc voltage produced from the AC-DC stage into the controlled dc voltage necessary to charge the EV battery. The Isolation provided to the battery of electric vehicle and the grid be achieved in one of two ways: either before the AC-DC stage install a transformer, followed by a DC-DC stage with no transformer isolation, to ensure isolation from the grid, or by using a high-frequency transformer housed inside an isolated DC/DC converter, as shown in Figs. 1.1 and 1.2.

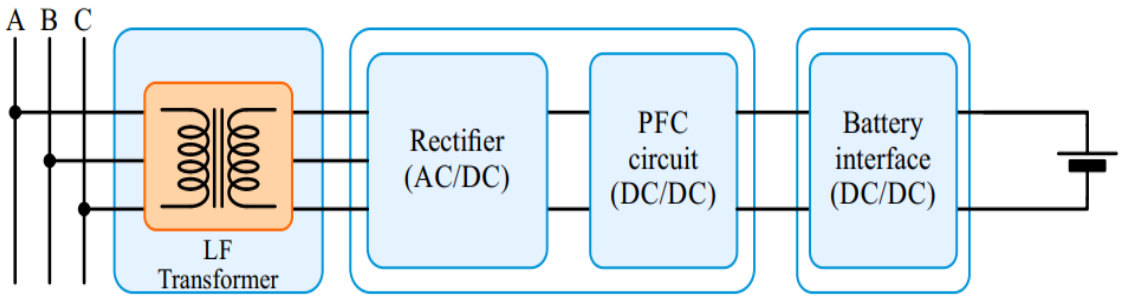

Figure 1.1 Non-isolated DC/DC converter connected Single module charger

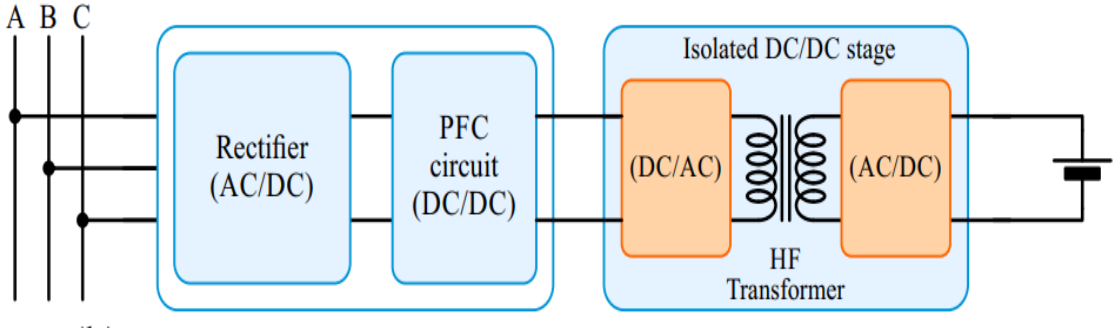

Figure 1.2 Isolated DC/DC converter connected Single module charger

Several similar modules are linked alongside to boost the P_O if a single-module charger is unable to provide the system's required power.

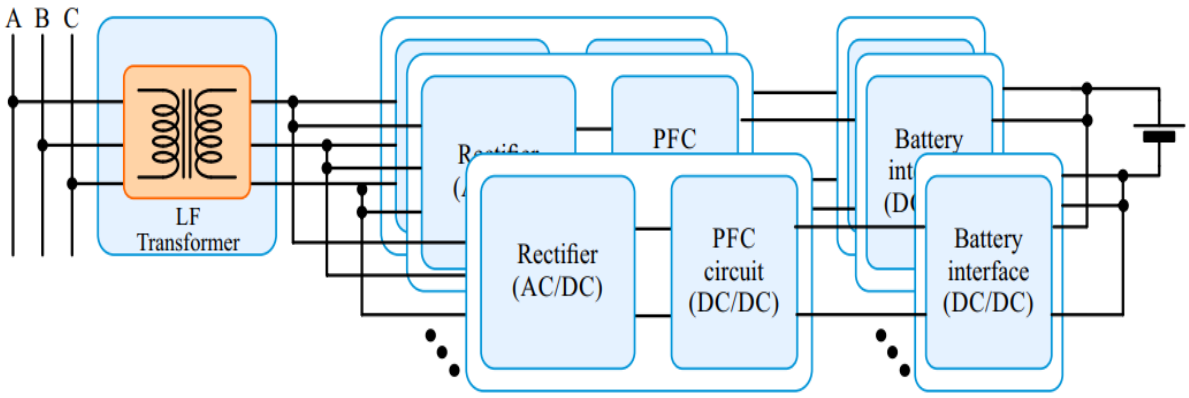

Figure 1.3 Multiple paralleled modules shown in Fig. 1.1

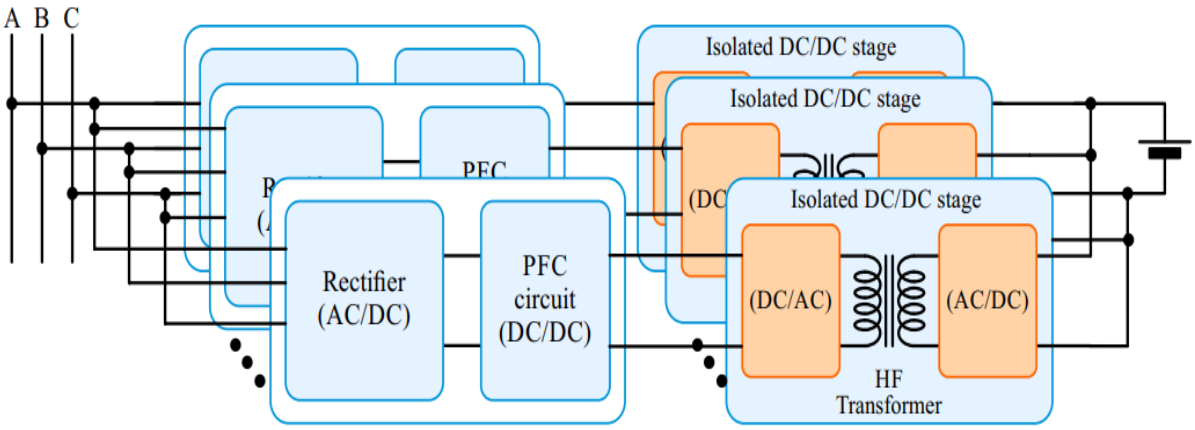

Figure 1.4 Multiple paralleled modules shown in Fig. 1.2

The batteries' charge acceptance capacity and the charger's wattage ratings, limit the amount of power transferred to the EV. The connector rates are specified by the standard, and the highest power capacity is currently supported by the CHAdeMO standard. Larger diameter cables are needed for high charging current in order to prevent overheating. Modern 50 kW fast chargers have cables that weight around 9 kg [4]. Weight of cable for 200 kW charging may be greater than the safe lifting limit for one person (22.7 kg) if the battery voltage remains at 500 V. Power transfer for greater voltage ranges is one technique for giving the vehicle more power and reducing cable.

EVs are probably creating issues for the utility because of growing adoption of EVs and the constantly rising charging rates. Uncontrolled EV charging may result in change in daily maximum load, overloading transformers and feeders, hastening transformer ageing, and increasing power losses [5]– [6]. Furthermore, the constant power consumption of the chargers' power electronics interface may negatively affect the stability of the system, lead to disturbance voltage, and reduce power quality [7].

1.2 CHARGING STATION CONCEPTS AND CONVERTER TOPOLOGIES

The interface between the distribution network and a three-phase AC bus operating at a line-to-line voltage of 250 V to 480 V in ac-connected systems is a step-down transformer. Every charger at the station is supplied by the AC bus, and every charger has a unique AC/DC stage. The number of conversion stages between the distribution network and the DC port of the EV or RES (such as a PV system or battery) is much higher using this approach. In an AC-connected system, the number of conversion stages makes system complex and increases costs while degrading system efficacy. Benefits of adopting the AC bus include the accessibility of AC switchgear and protective devices, the maturity and availability of rectifier and inverter technology, and the existence of standards and guidelines for power distribution AC systems. Standards for EV charging stations range between [8] and [9].

An Active front-end converter is utilized to generate a DC voltage for DC-connected equipment, offering energy-efficient method. Active front-end consists of transformer having lower frequency, an SST that performs isolation, voltage step-down, and rectification in one unit, and an LV (300 V–500 V) rectifier stage. DC voltage around 1000 V to fit the modern battery voltage range, which is around 400 V. Instead of using individual AC/DC converters, each charging unit is connected using a DC to DC conversion stage. In comparison to AC systems, the system efficiency is increased with fewer conversion stages. In addition to taking advantage of the load diversity brought on by changing capacities of EV battery, this gives an opportunity to greatly reduce the cost of system installation. It is made simpler to join the main grid and to become an island because of the single inverter's connectivity to it. The ability of DC distribution systems to utilize fractional power converters as a bridge connecting the DC bus and the automobile [10]– [11] is another possible benefit. These partial power converters improve conversion efficiency by merely processing the power supplied to the EV, thereby

lowering converter cost and rating. DC meters must be put in the DC-connected system to track the energy stored in battery. For DC-connected systems, the development of a standard and verified DC meter is required.

1.2.1 GRID-FACING AC/DC CONVERTERS

The grid and a regulated DC bus are connected via grid-facing AC/DC converters. A critical working need for these converters is high power aspect on the ac and dc sides, achieved through input current moulding and output voltage regulation [12], [13].

a). Bidirectional AC-DC Converters

The 3-phase active PWM converter with an LCL filter is the most popular grid-facing AC/DC converter. The output voltage of this boost-type converter is greater in magnitude than that of peak applied voltage. The PWM converter with 6 switches offers bidirectional power flow, minimal harmonic input current generation, and variable power factor (PF) adjustment. This architecture is commonly used in the most advanced DC fast chargers due to its straightforward construction, tried-and-true control techniques, and the accessibility of inexpensive IGBT devices with adequate current and voltage ratings [14].

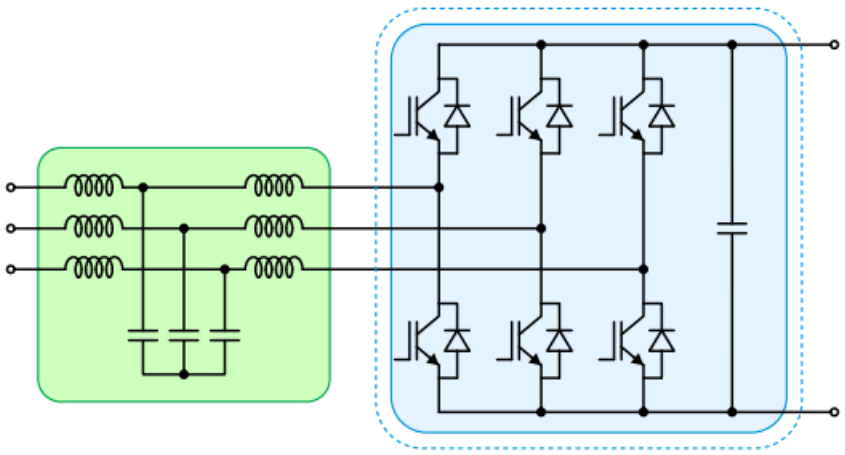

Figure 1.5 Three-phase PWM rectifier

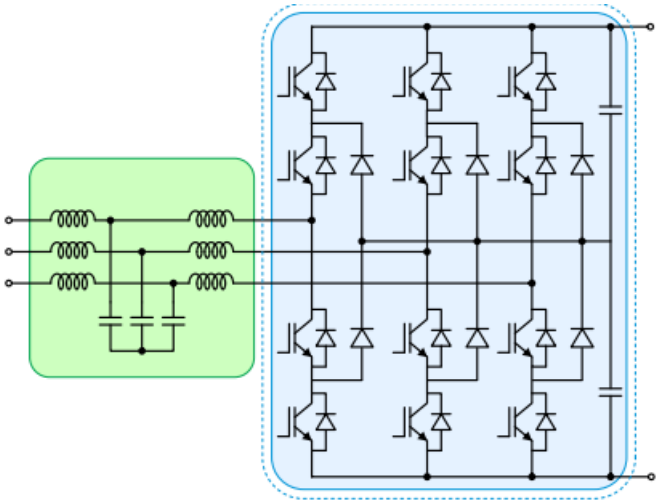

Figure 1.6 Neutral-point-clamped rectifier

b). Unidirectional AC/DC Converters

If just unidirectional power flow is necessary, a three-level solution called the T-type Vienna rectifier can be used. It shares some of the same limitations as 3-level converter, such as the desire for dc-link capacitor voltage stabilizing, but it also has all of their advantages. The Vienna rectifier has several limitations, including restricted reactive power regulation and unidirectional power flow. The range of reactive power that can be generated is constrained by the restricted modulation vector and primarily depends on the output voltage.

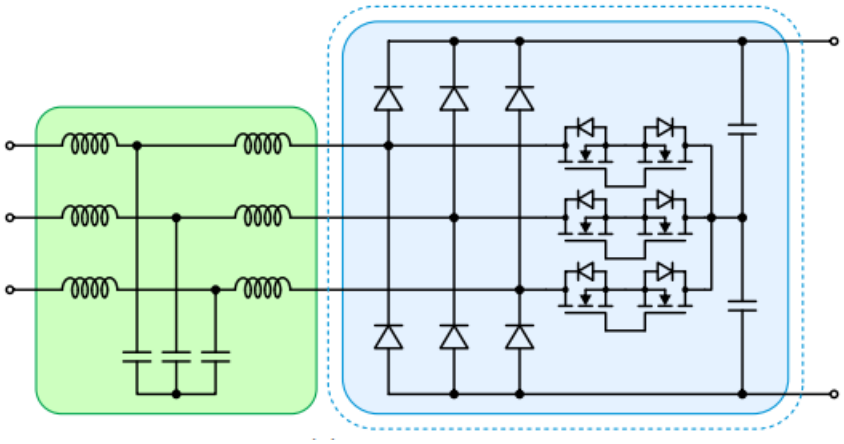

Figure 1.7 Vienna rectifier

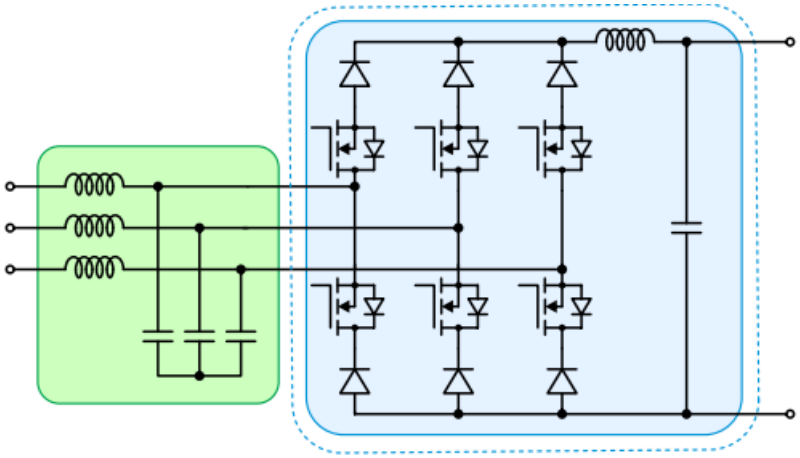

Figure 1.8 Buck-type rectifier

1.2.2 ISOLATED DC-DC CONVERTERS

After the AC-DC front-end, a DC-DC converter offers a connection to EV battery, RES, or battery energy storage. The Electrical isolation between EV battery and Grid is necessary to maintain the isolation because the EV's battery cannot be grounded. This makes sure that the battery's protection is not harmed throughout the battery charging procedure. A standalone DC/DC converter is capable of achieving this.

a). Unidirectional Isolated DC/DC Converters

When there is requirement of unidirectional power flow the phase-shift full-bridge (PSFB) converter, is one feasible implementation. While the converter is being controlled by phase-shift PWM, its operational switches run at ZVS turn-on[15]. This topology's principal flaws include its high output diode losses, the significant ringing across the output diodes brought on by the transformer L_m LCL resonance, the capacitance of the reverse biased diodes, and the turn-off losses in the operating switches. Snubber circuits, either active [15] or passive [16], can be employed to reduce system efficiency while preventing voltage overshoot and ringing. A current-fed PSFB converter is suggested in [17, 18] by relocating the L_O to the primary winding of the TF and simply linking an output capacitor to the diode bridge. Ringing and voltage overshoot are reduced using this technique, however the range of ZVS is greatly load-dependent. In [19] and [20], auxiliary circuits are suggested, and ZVS is maintained across a wide spectrum for charging EV batteries using trailing edge PWM. Equivalent supplementary circuits are

utilized in [21] to attain ZVS for an EV charger transitioning from no to full load using a PSFB converter.

The LLC resonant converter is another example of an isolated unidirectional DC/DC converter commonly used for battery charging. The output voltage of the converter can be altered by adjusting the switching frequency, which also affects the impedance ratio of the resonant tank to the equivalent load. Turn-off losses and transformer losses are minimized as a result of the LLC converter's usage of the magnetizing current to generate ZVS [22]. A very high efficiency can be attained by the LLC converter if the V_{in}/V_o is low [23]. The ZVS condition might not be stable across a large working range, and its low capacity for light-load power regulation has a negative impact on efficiency.

The resonant capacitor's requirement to tolerate high voltage stress at high power levels presents a new difficulty for the LLC converter, further complicating the element selection. To boost the power rating and lessen the burden on switching devices and resonating elements, an LLC converter with paralleled modules [25], a multilayer LLC converter [24], or a three-phase LLC converter [24] might be utilized.

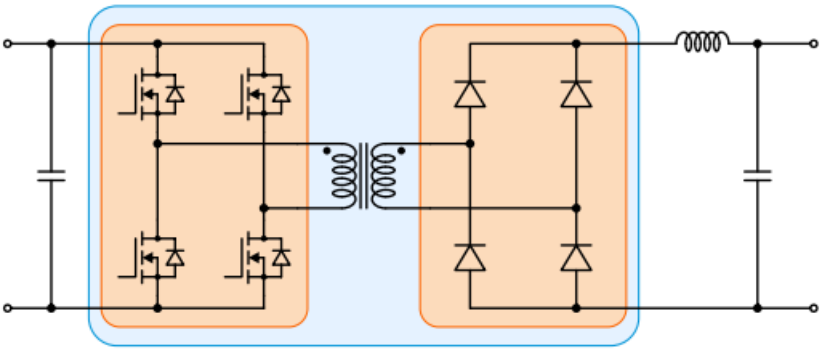

Figure 1.9 PSFB converter

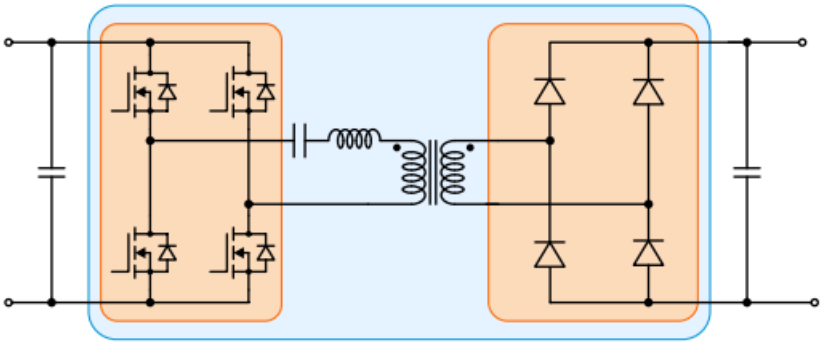

Figure 1.10 LLC converter

b). Bidirectional Isolated DC-DC Converters

EV charging applications may make use of a dual active bridge (DAB) converter. Bidirectional power flow may be needed due to large energy density, outstanding efficacy, buck and boost ability, lesser device stress, tiny filtering devices, and low susceptibility to component fluctuation [26]–[28].When the DAB converter was first introduced in 1991 [29], it was not widely employed because of the significant power dissipation and comparatively low switching frequency of the electrically powered semiconductor devices. The DAB converter has recently started to receive attention because to the abilities of the modern SiC and GaN-based power semiconductors and the developments in the nanocrystalline and polycrystalline soft magnetic materials, resulting substantial gains in converter effectiveness and power density [30]. The power transfer medium in the DAB converter is transformer leakage inductance, and the power flow is changed by adjusting the phase shift between the primary and secondary voltages. Due to its straightforward construction and ZVS operation, the DAB converter has been widely employed in isolated bidirectional DC/DC conversion applications [31, 32].

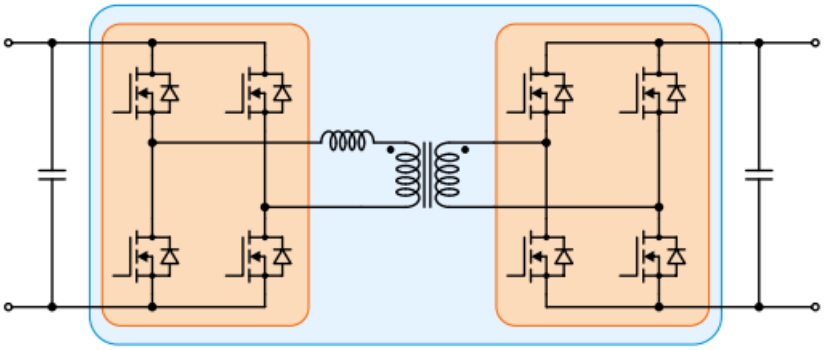

Figure 1.11 DAB converter

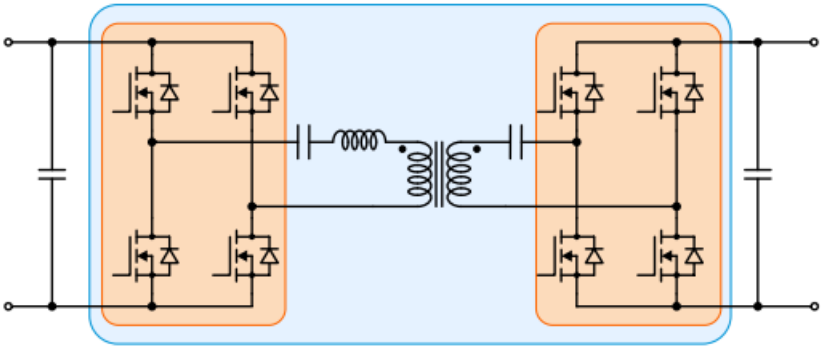

Figure 1.12 CLLC converter

The converter must operate with a broad range of gain in voltage and power for charging electric vehicle batteries because of the EV charging characteristics, where reactive electrical power can rise quickly and the ZVS is no longer true [33]. This creates a conundrum in leakage inductance modelling, where high leakage improves a large ZVS spectrum but degrades reactive power and leads to reduced efficacy [34]. Different modulation strategies have been developed to enhance performance over a broad working range.

1.2.3 Non-isolated DC/DC converters

By leveraging the isolation provided by an alternative power conversion stage in the charging battery system, such as the line-frequency transformer preceding the AC/DC front-end, it becomes possible to employ a non-isolated DC/DC converter. This allows for the provision of a circulating power supply to the vehicle battery. There are two reasons why this discussion encompasses bidirectional, non-isolated DC/DC converters. First, synchronous rectification makes bidirectional converters significantly more

efficient than unidirectional ones. Second, the control of non-isolated DC/DC converters is not made more challenging by their bidirectional performance, comparison to isolated DC/DC converters. Even though the discussions pertain to bidirectional converters, they also apply to equivalent unidirectional variants.

From the perspective of the battery, a boost converter serves as a relatively straightforward non-isolated architecture for interfacing with the battery, particularly since the battery voltage is often lower than the final output voltage of the AC/DC front-end. Although only one switch is required to carry current, the converter itself has a low power rating. Furthermore, a big inductor is needed to minimize the current ripple.

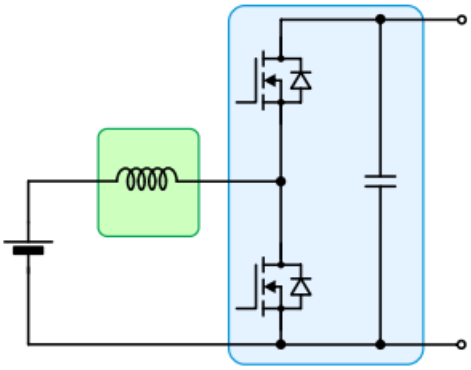

Figure 1.13 Boost converter

By connecting two or more phase legs together, a multi-phase interleaved boost converter can be used to enhance the current carrying ability and decrease the current ripple that the battery experiences. In this case, a three-phase interleaved boost converter is utilized, incorporating three distinct phase legs. Due to its uncomplicated construction, outstanding functionality, and adaptability to high power, this configuration has been thoroughly investigated in the published literature for electric vehicle (EV) charging applications [35], [36], [37]– [40]. According to [41], a prototype EV charger includes six phase legs that are interconnected in tandem to produce 30 kW. In [42], a 100 kW 3-phase interleaved boost converter is developed using discontinuous conduction mode (DCM). Nearly every switch are able to attain ZVS by permitting positive as well as negative current during a single switching cycle as the inductors are small enough. An optimized inductor design can lead to higher efficiency and smaller systems. By dividing

bus voltage into 2 parts and connecting them in series, the partial power notion is applied in [43] to build an interleaved boost converter that operates in DCM. It is feasible to employ switches with lower voltage ratings by connecting the converter to a portion of the bus voltage, potentially lowering losses. This method's disadvantage is the additional equipment and administration work required to balance the two DC bus voltages.

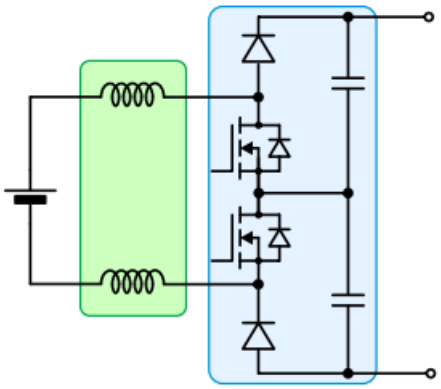

Figure 1.14 Unidirectional three-level boost converter

The boost converter [44] has a different topology from the 3-level boost converter and its bidirectional counterpart [45], which offers reduced harmonic content. The current distortion in the three-level boost converter, when the same inductor is used, is just one-fourth of the amount in the boost converter, indicating that a lighter inductor can be used to meet the current ripple standards. The 3-level boost converter can reduce the effectiveness and the dimension of the magnetic components. However, the battery system may suffer from the three-level boost converter's high levels of common mode noise electromagnetic interference (EMI). Furthermore, it is challenging to parallelize the three-level boost converters. When there exists a shift in phase related to phase leg of three-level boost, higher magnitude currents that circulate without interphase reactors are utilized in phase legs. Circulating electrical currents can be reduced in applications with high power requirements where several concurrent phase legs are required by simply switching each of the phases simultaneously [46], which avoids the inductor size from being reduced owing to interleaving, or by utilizing an integrated inductor that does so [47]. Due to its three levels, the 3-level boost converter is appropriate for connecting the batteries of an electric car to a bipolar bus.

1.3 THESIS OBJECTIVES

This thesis aims to investigate and analyze the application of an active front-end (AFE) converter feeding a dual active bridge (DAB) converter for electric vehicle (EV) battery charging. The objective is to propose a novel and efficient power conversion system that optimizes the charging process and addresses the specific requirements of EV charging infrastructure. The research will begin with a comprehensive literature review to understand existing EV battery charging systems, AFE converters, and DAB converters. The limitations and challenges of current charging techniques will be identified, and the potential advantages of the proposed system will be explored. A mathematical model of the converter system will be developed, and its performance will be analyzed, considering power factor correction, efficiency, voltage regulation, and harmonic distortion. An advanced control strategy will be designed to ensure optimal power transfer and efficient battery charging, considering techniques such as PWM. The developed control strategy and system model will be implemented in simulation software for performance evaluation, including parameters such as charging time, efficiency, voltage/current ripple, and harmonic distortion. Experimental tests will be conducted on a prototype to validate the simulation results and assess real-world performance. Finally, the thesis will conclude with a summary of findings, recommendations for further research, and an exploration of the implications of the proposed converter system for the future of EV charging technology.

1.4 THESIS ORGANIZATIONS

The thesis is organized as follows:

Chapter-1: This chapter provides the reader with an introduction of Electric Vehicle technology and background on converter topology and the importance of control structure.

Chapter-2: This chapter is about literature review of AC/DC and DC/DC converter-based Battery charging with integration of Grid.

Chapter-3: This chapter discusses about circuit description of Active Front End rectifier with the implementation of LCL filter and also discusses the closed loop control strategy of the AC/DC converter with simulation results.

Chapter-4: In this chapter, the EV battery charging under variable load scheme using Dual Active Converter is presented along with design specification and simulation results are discussed.

Chapter-5: In this the conclusion and future scope of the proposed system has been described.

CHAPTER-2

LITERATURE REVIEW

Macro Liserre et al. [48] Proposed a step-by-step method for developing a front-end three-phase active rectifier's LCL filter. The main objective is to achieve a high-performance front-end rectifier while reducing the switching frequency ripple at an affordable cost. The values obtained from an example LCL filter design have been used to create and test a filter. The experimental findings show how well the design process for the rectifier controller and LCL filter performed. A strong concordance between simulation and experimental results is another factor that supports the proposed approach.

Pablo F.S. Costa et al. [49] described the dual active bridge (DAB) converter with topological changes in the output. The generalized average model and the output current linearization model are two methods used to mathematically model the converter. The two methods are further contrasted, and the stronger model is used to construct the current and voltage controls for the DAB. The experiment's findings are then presented.

For battery charging applications, Alex V. Mirtchev et al. [50] provided a thorough design technique for a resonant dual active bridge (R-DAB) converter. The converter design process is based on unique operating points (UOPs) that result from an examination of two different control methods and is specifically adapted to the charging profile of a Li-ion battery. In order to prevent the resonant tank parameters from being overstated, a thorough flowchart is described that takes into account several design characteristics and the UOPs. The control method and design process are validated by the simulation results of a typical charger. Finally, a closed-loop control system is used to develop and assess a 1kW|30A laboratory prototype charger. The significance of the dual control approach is demonstrated by the analysis of the experimental findings, which also validates the suggested design methodology.

As a module construction for a battery charge/discharge tester, Sung-Jun Park et al. [51] presented a circuit architecture with a DAB converter and a non-isolated dc-dc converter. Also illustrates four series-parallel converter topologies and compares them to the scenario when a DAB converter is the only source of the output voltage. Examine the

features of automatic voltage balancing resulting from the discrepancy between the initial voltage and capacitance of the series-connected input capacitors. Additionally, perform a simulation analysis of the proposed system's features and conduct experiments employing super capacitors instead of batteries to confirm the technological viability and superiority of the suggested battery charge/discharge tester.

Jakka Venkat et al. [52] investigate the design and workings of a three-phase active rectifier-based PET. It is explained how a novel dq-vector-based control strategy for the rectification stage can keep the input side's power factor at unity, deliver a constant DC voltage at the rectifier output terminals under a variety of load conditions, and eliminate the need for phase locked loops (PLL) to determine the phase angle. A straightforward controller is used for DAB to generate the required DC-link voltage signal for the inverter circuit. In addition to having a constant voltage and a unity power factor, the design described can also allow for bidirectional power transmission. Results from simulations performed with PSCAD and EMTDC are displayed to support the proposed topology and controller.

Saran Chaurasiya et al. [53] describe a bidirectional off board rapid EV charging system with voltage and current stress reduction for a wide voltage spectrum. It has an integrated two-stage power conversion system. A complete circuit calculation of a DC-DC stage with DPS control is presented in this context to check the location of a safe working area with lower voltage stress. The discovered operating zones are subjected to the particle-swarm optimization technique in order to choose the converter control settings with the best current stress in conjunction with the lowest voltage stress. A 7.2 kW system is constructed and simulated in MATLAB/Simulink. A 3.3 kW laboratory prototype is developed to test the established operating points with a diverse battery voltage and spectrum and under different source and loading conditions.

Lingxiao Xue et al. [54] conducted an analysis and used sinusoidal charging on the basis of a two-stage battery charging system with a Full Bridge (FB) AC-DC stage and a Dual Active Bridge (DAB) DC-DC stage. More investigation reveals that converter loss is responsible for the increased DC link capacitance and ripple power imbalances. Therefore, it is identified how converter loss impacts the ripple power balance in order to further reduce the DC link capacitance. Based on this research, a feedback control on the

DC link voltage ripple is recommended. The effectiveness of the suggested techniques is confirmed in both Si-based and GaN-based charging systems.

Implementing ZVS soft switching of dual active bridge isolated converters (DAB) using a single phase shift control technique is the main emphasis of Xu Fei et al.'s work [55]. First, a thorough theoretical study and mathematical simulation of the single phase shift (SPS) are built. The process of ZVS switching into dead-time mode can then be created in accordance with the SPS's operating principle. It can discover the prerequisites for ZVS soft switching through a thorough examination. The simulation results show that when the requirements are met, ZVS soft switching is feasible. The theoretical analysis is then validated using a simple experiment bench.

Saran Chaurasiya et al. evaluate the performance of SPS (single phase shift) control for a dual active bridge. [56]. On the DSP, the SPS control is applied with both internal and external phase shifts. Furthermore, a high-power-density dual active bridge (DAB) DC-DC converter design approach is discussed for EV charging. The development and testing of a 6.6 kW prototype with SPS modulation and internal and external phase shift control A loss model is also built for comparing the losses encountered in the two phase changes. SPS modulation using both forms of phase shift is compared in simulations and tests.

In a freestanding PV/battery dc power system, R. D. Bhagiya et al. [57] propose a pulse width modulation-based two-loop PI control method to manage the load bus voltage magnitude in the presence of a constant power load. Frequency domain measurements are used to assess the stability of the inner loop and outer loop controllers. By applying a DC-DC boost converter and the incremental conductance technique, the solar array's instantaneous maximum power is extracted. MATLAB/Simulink software is used to validate the effectiveness of the suggested technique under various load scenarios and solar irradiation levels.

2.2 Conclusion

Several significant conclusions can be drawn from the literature review on grid-connected active front-end rectifier fed dual active bridge converters for EV battery

charging. First off, the efficacy and power quality of these converters show a noticeable improvement. They guarantee effective and clean power transfer between the grid and the EV battery with their high conversion efficiency, low total harmonic distortion, and power factor correction. The dual active bridge converter's capacity to offer bidirectional power flow is another crucial feature. With the help of this technology, energy can be transferred from the grid to the EV battery during charging and back to the grid during V2G operations. The flexibility and adaptability of EV charging systems are increased by this bidirectional power flow, enabling vehicle owners to use grid services and efficiently manage their energy.

Several obstacles still exist, though. To overcome system uncertainties, these involve creating sophisticated control techniques, managing power flow while many EVs are present, and tackling grid integration problems including synchronization and power quality control. To further improve the performance of grid-connected active front-end rectifier-fed dual active bridge converters, future research should concentrate on overcoming these issues.

CHAPTER-3
ACTIVE FRONT END RECTIFIER WITH LCL FILTER

3.1 Introduction

Pulse width-modulation (PWM) voltage-source converters (VSCs) are consequently widely used as active front-end converters in low-voltage drives as a result of emerging applications including regenerative energy sources, rising energy costs, and tight international grid requirements. Other benefits of such a converter architecture include the ability to ride through and alter the dc-link voltage as well as sinusoidal input currents, an controllable PF at the PCC, and ride-through ability.

The simplest filter design between a PWM voltage source converter and the grid is an inductance. For medium- and high-power converters (S>x kVA), a pure inductive filter is not used due to the constrained maximum dc voltage and poor dynamic action of a converter with common switching frequencies, as well as the high prices and large inductance [58], [59].

The use of an LCL filter is a desirable approach to solving these issues. The LCL filter's superior harmonic attenuation makes it possible to meet the harmonic limits indicated in general by using lower switching frequencies. It is difficult to design the LCL filter components to meet the specified maximum current harmonics. There is currently no accurate design methodology based on the grid's harmonic current constraint.

Reference [60] provides a design process that uses the trial-and-error approach. The design process is complicated, in particular, by the choice of initial values for the converter current ripple and the filter capacitance absorbed reactive power. Additionally, it does not address the design of the converter-side inductance for a certain converter current ripple. In [61]– [62], basic analytical equations are provided for calculating the upper limits of the filter inductance, filter capacitance, and converter current ripple. According to reference [60], the filter inductance is designed using the maximum converter current ripple, and the filter capacitance is selected using reactive power. [62] presents the fundamental requirements for an LCL filter design based on the filter attenuation factor for the grid current harmonic at switching frequency.

3.2 Circuit Description

The PWM control approach can be used to make a rectifier flexible. When the input power factor needs to be made perfect, the rectifier with this control is typically used as an active front-end rectifier. The general-purpose three-phase PWM rectifier is depicted in Fig. 3 and is made up of six power electronic switches, anti-parallel diodes connected to each switch, inductors and capacitors connected to each phase of the AC side to reduce input current ripple, and one capacitor on the DC side to reduce output voltage ripple.

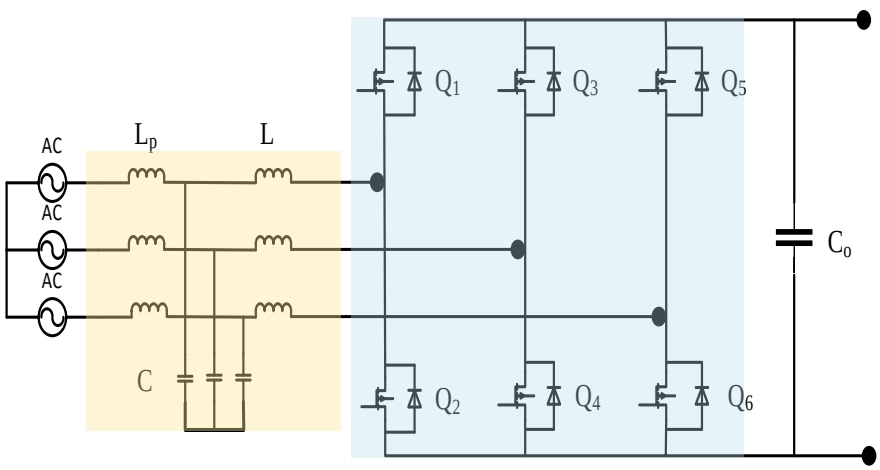

Figure 3.15 Active Front End Rectifier with LCL Filter

Two major challenges that are related must be resolved in order to effectively regulate the DC-bus voltage. The first one has to do with brief changes in the active power drawn that cause transient fluctuations in the DC-bus voltage. The second problem has to do with double-line frequency (2 ω) ripples in the dc-bus voltage that are present in single-phase ac systems by default [58]. Since these ripples may contribute a third harmonic component, or h3, to the grid current during steady-state operation, they may have an impact on the performance of the control system.

3.3 LCL Filter Design

LCL filters are superior to LC filters because they require fewer rated inductors and capacitors to minimize distortions from a voltage or current by the same amount. Choosing the right inductance and capacitance values for LCL filters entails achieving the correct filtering properties. LCL filters are specifically designed to reduce the absorption of harmonic current by power converters when the input stage is a rectifier. Frequency converters are used in UPS systems, motors, etc. For the most part, they are made up of reactors and capacitors that are coupled in parallel-series to reduce the THD of rectifiers.

When selecting LCL filters, the converter's absorbed current has to be taken into consideration. In the case of converters with extremely low power ratings, a special LCL filter can possibly be used to supply numerous converters, but only when they all begin and end at the same time. If the system offers many converters that operate and stop independently, harmonics will not be effectively filtered. Each converter in this case needs to be equipped with its own LCL.

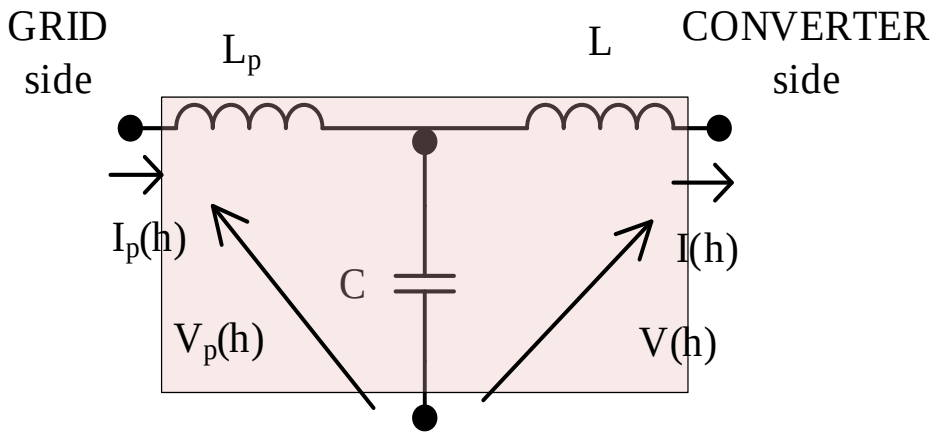

Figure 3.2 LCL Filter

The methodical steps that follow can be used to create the LCL filter.

1) On the converter side, select the necessary current ripple.
   Create the inner inductor L. Using the index α for the relationship between the two inductances, the value of the outer inductor may then be calculated as a function of L.

$$L_p = \alpha L \tag{3}$$

2) Choose the reactive power absorbed at the specified parameters. determine the value of the capacitor. Suppose that is expressed β as a % of the reactive power absorbed under particular circumstances.

$$C = \beta C_n \tag{3.1}$$

$$C_n = \frac{1}{\omega_n Z_n} \tag{3.2}$$

3) Design the outer inductor after deciding on the desired current ripple reduction. The filter's damping and computed losses-neglecting ripple attenuation,

$$\frac{I_p(h)}{I(h)} \approx \frac{1}{|1+\alpha(1-\sigma\beta)|} \tag{3.4}$$

$$\sigma = LC\omega_S^{\,2} \tag{3.5}$$

where σ is a fixed value. The desired attenuation should be multiplied by a factor that takes into account the losses and the damping before using (15) to compute. A different attenuation level or alternative value for the absorbed reactive power should be chosen as per step 2 if the total of the two inductances does not adhere to the criteria.

4) Verify the resonant frequency obtained

$$\omega_r = \sqrt{\frac{L_t}{LL_pC}} \tag{3.6}$$

which can be written, considering (7), (13), and (14), as

$$k = x\sqrt{\frac{1+\alpha}{\alpha\beta}} \tag{3.7}$$

$$\text{Where} \quad x = \frac{1}{\omega_s\sqrt{CL_p}} \tag{3.8}$$

x is a fixed value. Condition (c) imposes a restriction on the resonant frequency. If this is incorrect, either the attenuation returned in step 3 or the absorbed reactive power returned in step 2 should be modified.

5) Set the damping to the aforementioned condition (d). The filter's impedance is 0 at the resonant frequency. To prevent oscillation, the damper inserts an impedance at this frequency. Since the series capacitor impedance at the resonant frequency is of a similar order of magnitude, the damping value is set accordingly [63]. The design process loops back to step 3 to increase the multiplication coefficient, which takes into account the reduction in filtering action due to losses if the filter attenuation is insufficient. If this is insufficient, step 2 of the design process should be repeated, this time choosing a larger number for the reactive power.
6) Check the filter attenuation using different switching frequencies and different load circumstances.

3.4 Closed loop control

To accomplish independent control of the active and reactive power components in three-phase systems, the decoupled dq control technique is frequently utilized. This control strategy enables precise management of the DC voltage while permitting the needed active power transfer in the case of a three-phase active front-end rectifier with DC voltage sensing.

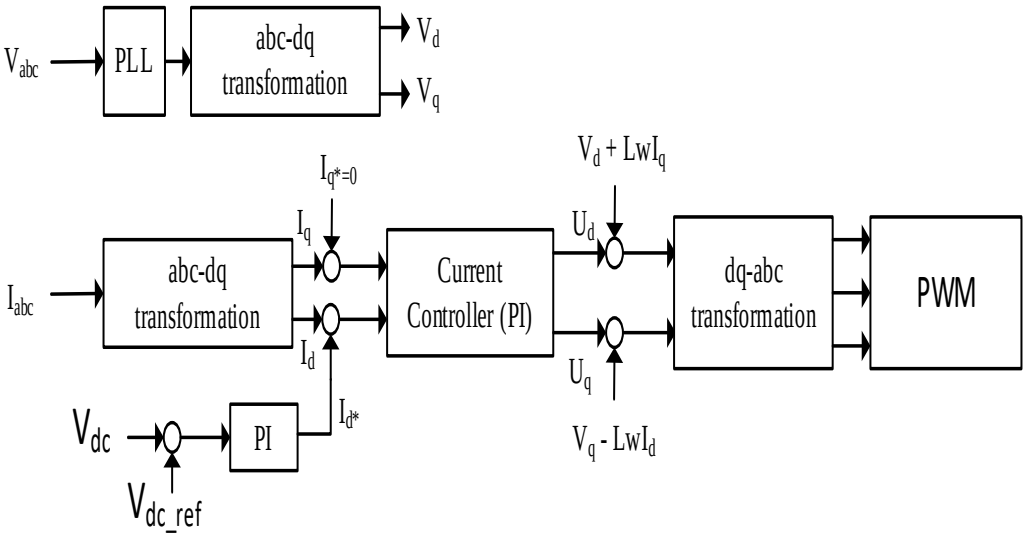

Figure 3.3 Decoupled DQ Control

The Clarke transformation is used to convert the three-phase AC input voltages from the time domain to the stationary reference frame. The three-phase voltages are transformed into a two-coordinate system made up of voltages along the d- and q-axes.

The Park transformation is then used to further transform the altered d-axis and q-axis voltages from the Clarke transformation into a rotating reference frame. This transformation generates two control signals, Vd and Vq, and lines up the d-axis with the DC voltage reference.

Based on the planned operation, the control algorithm generates reference values for the d-axis and q-axis control signals. By properly controlling the active power transfer, the main goal is to maintain the DC voltage at the intended set point.

The d-axis control signal (Vd) is in charge of controlling the DC voltage level in the decoupled dq control system. The rectifier regulates the active power transfer to keep the DC voltage at the appropriate set point by adjusting the d-axis control signal. On the other hand, the reactive power component is controlled by the q-axis control signal (Vq), which is also used to meet other system requirements like power factor correction and harmonic abatement.

PWM (pulse width modulation) signals are then created from the control signals (Vd and Vq). These PWM signals control how the rectifier's power electronic components (such as IGBTs) are switched on and off, producing the desired output voltage and current waveforms.

To make sure the rectifier's performance satisfies the necessary goals, a feedback loop is built. Any deviations from the required values are fed back to the control algorithm by the rectifier, which continuously monitors the output voltage and current. In order to maintain the stability and regulation of the DC voltage, the control algorithm modifies the d-axis and q-axis control signals correspondingly.

The three-phase active front-end rectifier achieves precise DC voltage regulation while independently managing the active and reactive power components by combining decoupled dq control with DC voltage sensing. With the help of this control strategy, the rectifier may adapt to different system needs and continue to run steadily in the direction of the desired goals.

In conclusion, a three-phase active front-end rectifier may be controlled effectively using the decoupled dq control technique in conjunction with DC voltage monitoring. The rectifier continuously modifies its operation to maintain a constant and regulated DC voltage while independently managing the active and reactive power components as necessary through PWM signal generation and feedback loops. This control strategy ensures that the rectifier's performance is in line with the required goals and permits exact power transfer.

3.5 Simulation Results

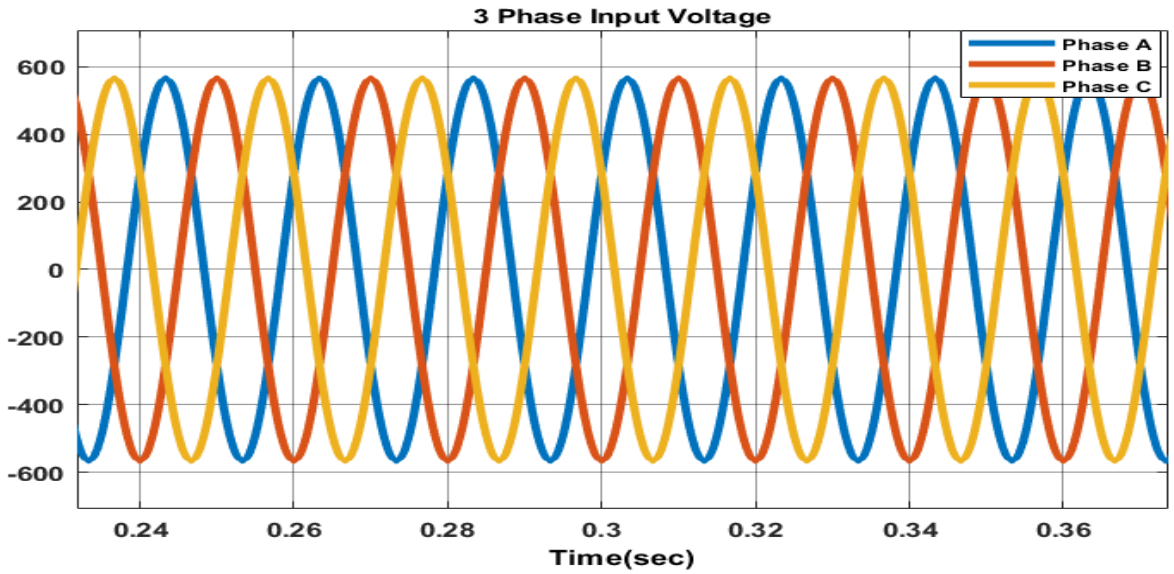

Figure 3.4 Three phase Input Current (Grid)

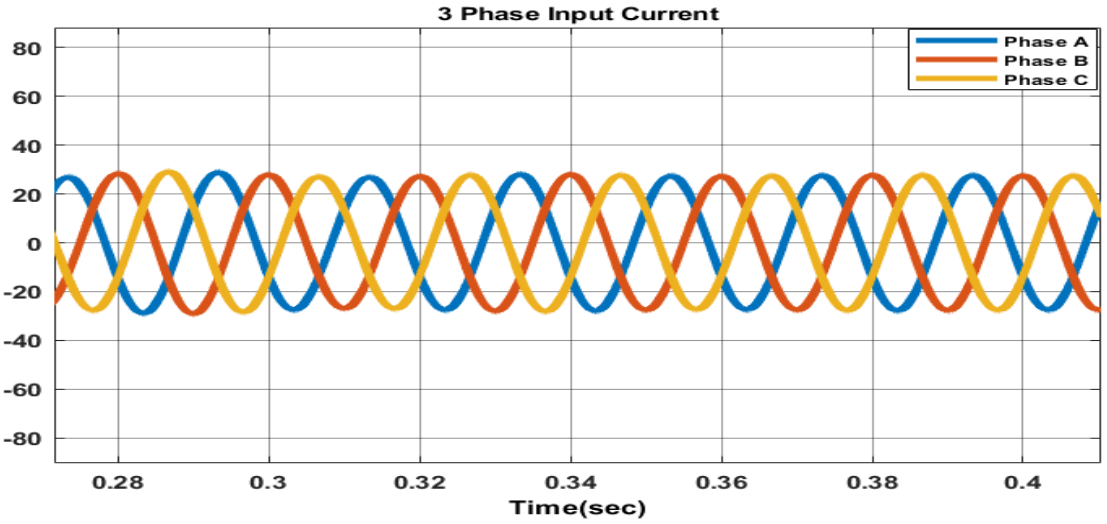

Figure 3.5 Three phase Input Current (Grid)

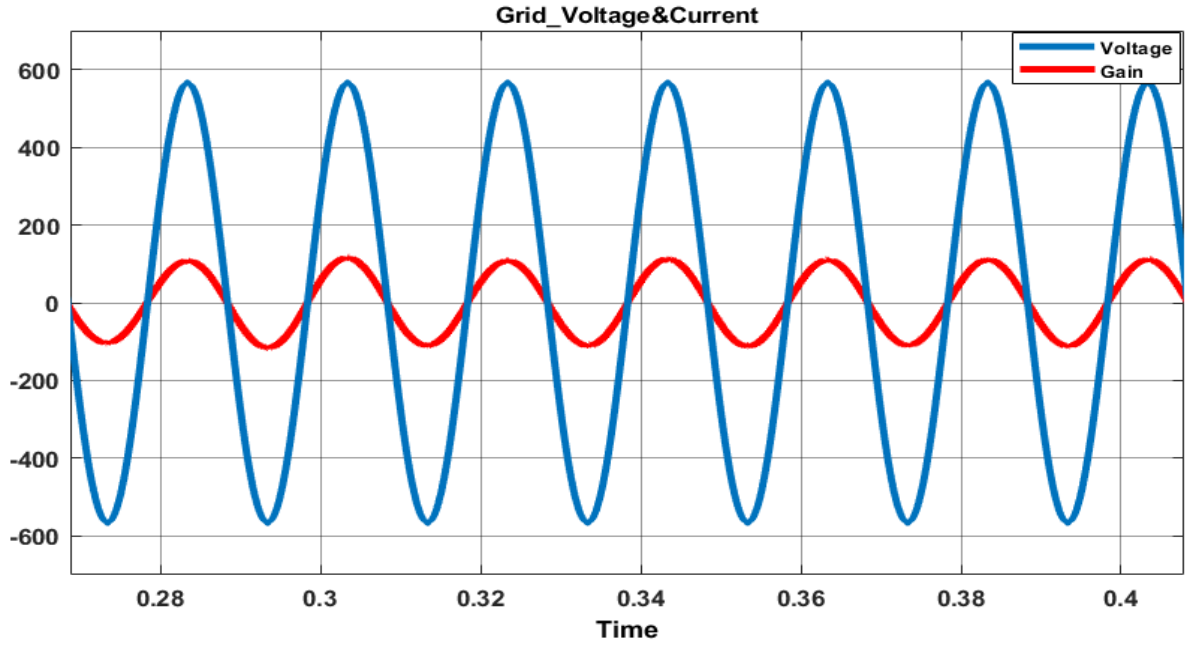

Figure 3.6 Unity Power Factor Maintained by Grid Voltage and Grid Current

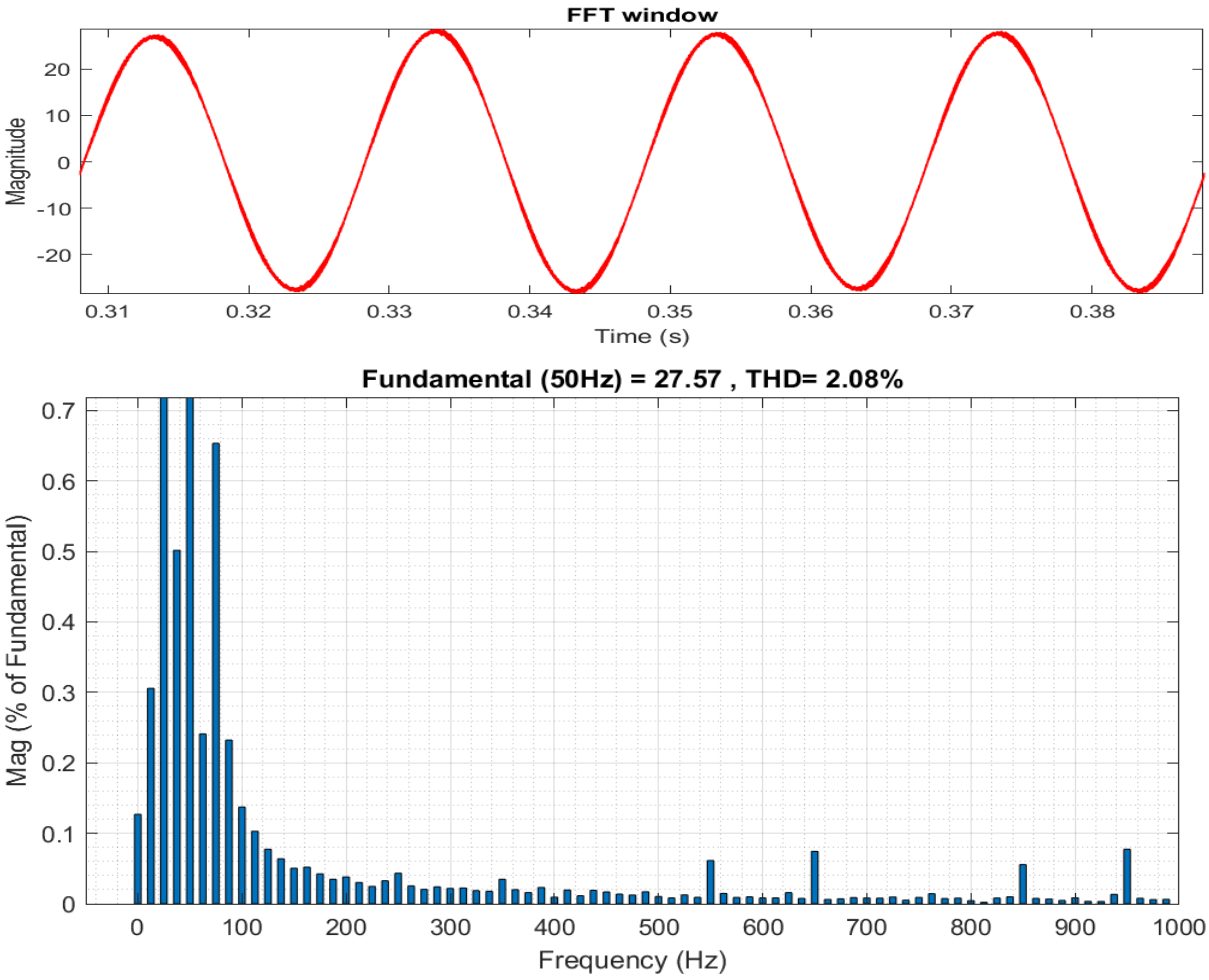

Figure 3.7 THD in Input Current (Grid)

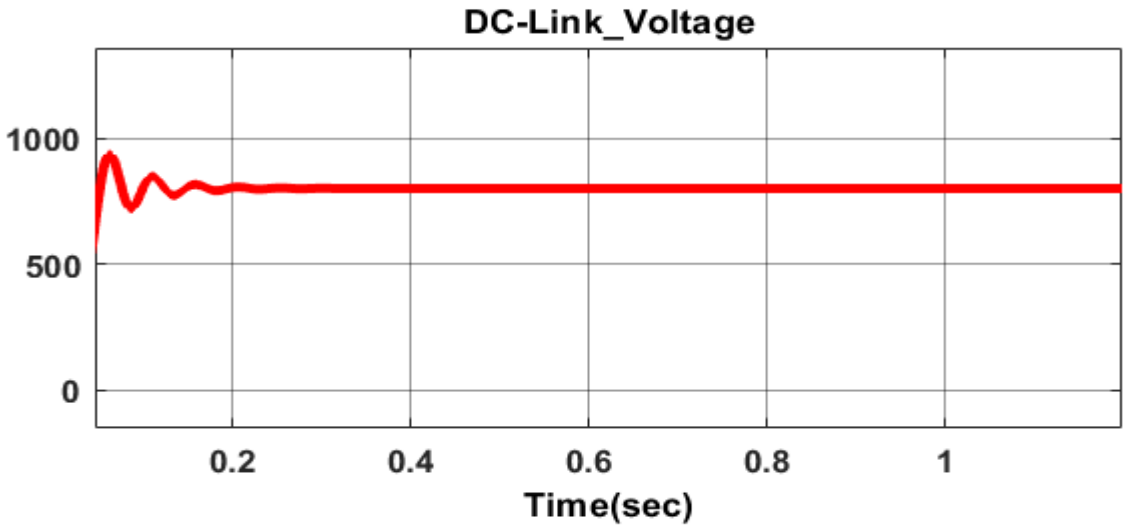

Figure 3.8 DC-Link Voltage

3.6 Conclusion

The design of the LCL filter and the closed-loop control of the active front-end rectifier are presented in this chapter. The three-phase 440 V input voltage is what the AC-DC converter is intended for, as illustrated in Figs. 3.4 and 3.5, which also depict the three-phase current. Increased efficiency, lower voltage drops, and capacity optimization are advantages of power factor improvement. As illustrated in Fig. 3.6, the power factor must be kept close to unity for the AFE rectifier to operate effectively. Additionally, to obtain a clear vision, the current must be multiplied by a gain of 4. According to IEEE standards, the THD must be less than 5%. Since the THD value in Fig. 12 is about 2.08%, the approved LCL filter parameters are precise. The DC-Link voltage should retain its magnitude even after switching several loads in parallel because of the decoupled DQ control. The DC-Link voltage is kept at 800 volts throughout the charging process, as shown in Fig. 3.8.

CHAPTER-4
DESIGN AND CONTROL OF DUAL ACTIVE BRIDGE CONVERTER

4.1 Introduction

The use of bidirectional dc-dc converters has substantially expanded with the quick development of distributed resource interfaces, electric vehicles, energy storage systems, and uninterruptible power supply systems. because of characteristics like as its high power density, gentle switching prowess, galvanic isolation, and lack of passive components. Dual active bridge (DAB) converters are a more common type of bidirectional buck/boost converter than other conventional models. The significant harmonic production at integer multiples of the high-frequency switching DAB converter's own significantly high fundamental switching frequency has an impact on the power grid. To improve the output voltage and current quality, a DAB converter is cascaded with an LC output filter.

Power density and system efficiency are two key requirements for a converter in a DC charging station. Low-switching-frequency operation allows for smaller magnetics. By increasing the bus voltage to enable rapid charging, more power may be transported at the same current level. As a result, the converter uses less copper and has a higher power density. In order to save money and reduce the thermal solution, the converter must also be very efficient. This more efficient thermal design directly translates into a smaller and more efficient heat sink, increasing the converter's power density. By increasing the bus voltage to enable rapid charging, more power may be transported at the same current level. As a result, the converter uses less copper and has a higher power density.

The lead-acid or lithium-ion batteries that are frequently used in EV charging stations must be able to easily interface with the DC/DC converter. Additionally, the DC/DC converter must be able to provide galvanic isolation between the high- and low-voltage sides and the necessary voltage conversion between them. The dV/dt capability of conventional switching devices, or more properly, the speed at which they can switch high voltages, is limited. Due to the device spending more time in the switching transition, the delayed ramping process increases switching loss. The longer changeover periods also result in a greater requirement for dead time in the control system to prevent shoot-

through and shorts. In more recent switching semiconductor technologies, such as SiC and GaN devices with great electron mobility, the answer has been found. This reference design demonstrates the potential advantages of TI's SiC gate driver technology in terms of efficiency and power density by combining SiC MOSFETs with it.

The following four popular topologies were evaluated for analysis.

• Phase-shifted, full bridge
• LLC resonant converter
• Dual-active bridge in CLLC mode
• Single-phase, dual-active bridge

The dual-active bridge was selected for use in this reference design based on this study because it is simple to operate in both directions, has a modular construction, is competitively efficient, and has higher power density values than other competing topologies. The primary emphasis of this reference design lies in addressing the difficulties associated with developing a high-power, dual-active-bridge DC/DC converter intended for an electric vehicle (EV) charging station.

4.2 Circuit Description

As shown in Fig. 4.1, the bidirectional DAB converter is constructed using two active bridges coupled by a high-frequency transformer. Power flow between these two bridges is analogous to power flow in a power system between its two voltage buses. Four MOSFET switches, anti-parallel freewheeling diodes, and snubber capacitors make up each active bridge.

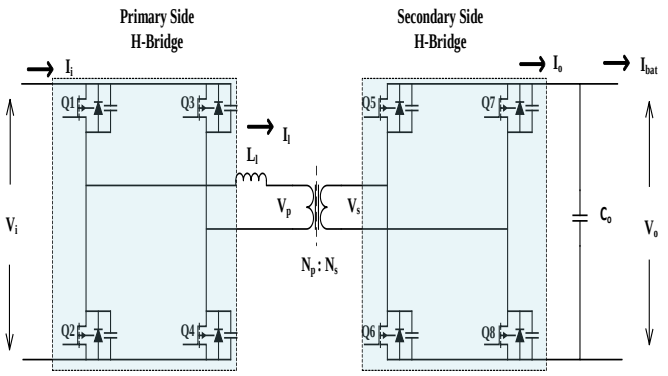

Figure 4.1 Bidirectional Dual Active Bridge Converter

There are three possible methods for controlling the DAB converter: switching frequency, duty ratios of switching devices, or phase shift between the two bridges. The efficacy and simplicity of the phase-shift control method led to its adaptation in this study. Each active bridge is operated at a predetermined duty cycle (50%) in order to generate high-frequency square waves at the transformer terminals. The phase shift between these two square waves can be changed, and the sign of the phase shift has an impact on the power flow.

.

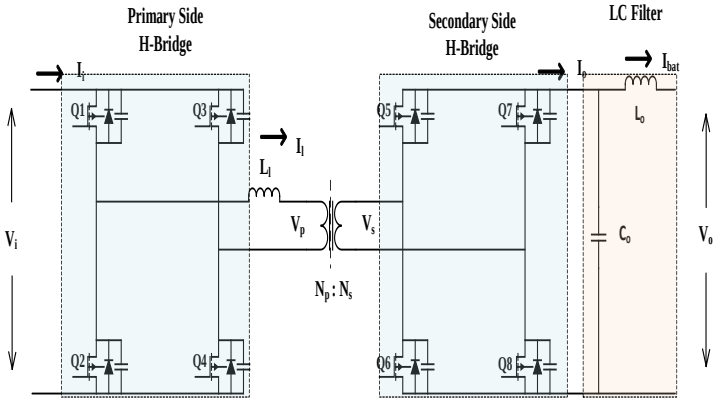

Figure 4.2 Bidirectional Dual Active Bridge Converter with output inductance

The transformer leakage inductance and, if necessary, an additional inductor connected in series are contained in the Ll, which is the main part of power transfer [63]. The output inductor Lo and capacitor Co comprise the DAB converter's overall structure, which is shown in Fig. 4.2. It has been observed that when the inductance value increases, the ripple of the output current gets smaller. This is made clearer when the output capacitor is also reduced, aiming for greater power density at the expense of volume. The traditional DAB converter architecture has a sizable current ripple of roughly 40% without an output inductor. Reduced current ripple values, which place less stress on batteries in terms of internal temperature, are the main reason for extending their service life.

4.3 Design Consideration

When designing the power stage of a dual-active bridge, it is crucial to take into account several factors and considerations. The most important considerations are the design of the transformer, output capacitor, SiC MOSFETs used, transformer design, suggested ZVS range of operation, planned phase shift, switching frequency, and leakage inductor.

4.3.1 Leakage Inductor

$$L_l = V_i V_0 \frac{nd(1-d)}{2P_o F_{sw}} \tag{4}$$

$$i_{l1} = 0.5(2\phi - (1-m)\pi) I_n \tag{4.1}$$

$$i_{l2} = 0.5(2m\phi + (1-m)\pi) I_n \tag{4.2}$$

Where, m is voltage transfer ratio

$$m = \frac{V_o}{N V_i} \tag{4.3}$$

4.3.2 Phase Shift

The shift in phase of converter is influenced by the leaking inductor. Equation (5) yields the phase shift necessary for the necessary power transfer.

$$\phi = \frac{\pi}{2}\left(1 - \sqrt{1 - \frac{8 \times F_{sw} \times L_l \times P_o}{N V_i V_o}}\right) \tag{4.4}$$

4.3.3 Output Capacitor

For a given value of phase shift, the leakage inductance grows, increasing the quantity of capacitance required to maintain the voltage ripple at a predetermined level in compliance with the system specification.

$$R = \frac{V_o^2}{P_o} \tag{4.5}$$

$$C_O \frac{dV_o}{dt} = \frac{V_i}{X_{Ll}} \phi\left(1 - \frac{\phi}{\pi}\right) - \frac{V_o}{R} \tag{4.6}$$

In order to ensure that the ripple of the output voltage remains below 5%, the output capacitor was carefully chosen.

4.3.4 Resonant Frequency

$$f_{res} = \frac{1}{2\pi\sqrt{L_l C_s}} \tag{4.7}$$

4.3.5 Zero Voltage Switching

When considering the principal H-bridge, Q1 and Q4 switch on and off simultaneously. Here, the same Vds value is used to simultaneously charge or discharge the Cs of Q1 and Q4. The input and output voltages, switch capacitances, and leakage inductance are all components of the resonant process.

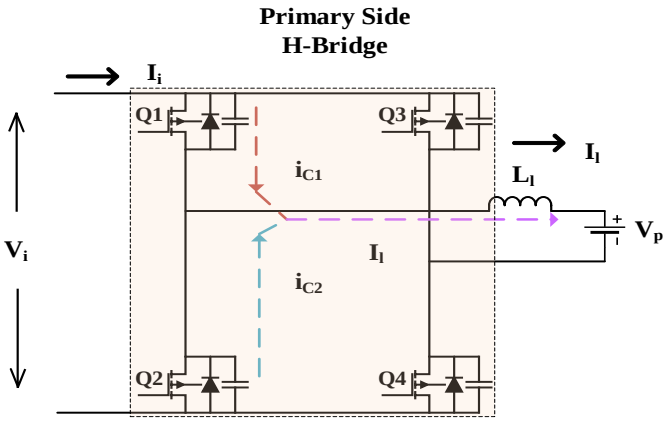

Figure 4.3 ZVS Transient Process

The ZVS transitory process takes place when Q1 and Q4 are off but Q2 and Q3 are not yet on. Vi supplies power for the ZVS process once the input voltage source releases current. However, as the current progressively reverses polarity, Vi is showing signs of energy depletion. The input voltage source's power output or dissipation is actually zero, but as will be shown later, it still affects the ZVS transition time.

The relationship between the capacitance voltage and inductor current is depicted in (9) through (14), assuming that vc is the voltage across the output capacitance of Q1.

$$V_i = V_{C1}(t) + V_{C2}(t) \tag{4.8}$$

$$v_C = V_{C1}(t) \tag{4.9}$$

$$I_i(v_C) = i_{C1}(v_C) - i_{C2}(V_i - v_C) \tag{4.10}$$

$$I_l(v_C) = i_{C1}(v_C) + i_{C2}(V_i - v_C) \tag{4.11}$$

$$i_{C1}(v_C) = C_1(v_C)\frac{dv_C}{dt} \tag{4.12}$$

$$i_{C2}(v_C) = -C_2(V_i - v_C)\frac{d(V_i - v_C)}{dt} \tag{4.13}$$

To acquire the energy consumed by the voltage source in the circuit, the charge travelling through the inductor and DC source during the transient process is necessary, and this charge is

$$Q_{I_l}(v_C) = \int_0^v (C_1(v_C) + C_2(V_i - v_C))dv_C \tag{4.14}$$

$$Q_{I_i}(v_C) = \int_0^v (C_1(v_C) - C_2(V_i - v_C))dv_C \tag{4.15}$$

Consequently, the amount of energy wasted during the transient process in the input and output voltage sources is

$$E_{diss}(v_C) = -Q_{I_i}(v_C)V_i + Q_{I_l}(v_C)V_p \tag{4.16}$$

The total initial energy stored in the inductor and H-bridge is

$$E_{init} = \frac{1}{2}L_l I_l^2(0) + 2E_S(0) \tag{4.17}$$

The remained energy in H-bridge and inductor at the end of ZVS is

$$E(v_C) = \frac{1}{2}L_l I_l^2(v_C) + 2E_S(v_C) = E_{init} - E_{diss}(v_C) \tag{4.18}$$

Combining (17) and (19), one can determine the inductor current based on a specific capacitor voltage, which is

$$I_l(v_C)=\sqrt{I_l^2(0)+\frac{2}{L_l}(2E_S(0)-2E_S(v_C)-Q_{I_l}(v_C)V_p+Q_{I_i}(v_C)V_i)} \tag{4.19}$$

To obtain the relationship between vc and inductor current as the ZVS transition time, we must simplify (9)–(14).

$$\frac{(C_1(v_C)+C_2(V_i-v_C))dv_C}{I_l(v_C)}=dt \tag{4.20}$$

The inductor current can also be written as a function of vc based on (20). The transient process charges Q1's output capacitance. As a result, the transition time grows from 0 to tZVS, while vc increases from 0 to Vi. Then,

$$t_{ZVS}=\int_0^{t_{ZVS}} dt=\int_0^{V_i}\frac{(C_1(v_C)+C_2(V_i-v_C))}{I_l(v_C)}dv_C \tag{4.21}$$

The charge flowing through C1 and C2 is the same throughout the entire transient phase. Therefore, as indicated in (23), the total charge flowing through the input voltage source is 0, in accordance with (15)–(16).

$$\int_0^{V_i} Q_i(v_C)dv_C=0 \tag{4.22}$$

$$E_S(0)=E_S(V_i) \tag{4.23}$$

The least amount of inductor energy feasible is needed for the ZVS transient approach, which is

$$\frac{1}{2} L_l I_l^2(0) \geq 2Q_S(V_i)V_p \tag{4.24}$$

4.3.6 Switching Frequency

The efficiency and power density of a power converter are significantly influenced by the choice of switching frequency, which serves as a crucial design element. The selection of switches for the power stage is primarily determined by the input and output voltage levels. SiC MOSFETs are used in the power stage, which results in exceptionally high switching frequencies. Smaller magnetics are made possible by operating at higher switching frequencies, which improves the thermal situation and boosts the power density of the converter. The permissible heat sink solution and transformer size must therefore be traded off in order to determine the switching frequency for a given efficiency target. Second, using a high switching frequency lowers efficiency if the MOSFET's output capacitance (Ecoss) is particularly large, as it causes significant switching losses at low loads. Implementing the control loop bandwidth is influenced by the selection of the switching frequency as well. The switching frequency for this application was chosen to be 100 kHz after considering all of these aspects.

4.3.7 Transformer Selection

A power supply system's size is significantly influenced by transformers and inductors. The efficiency of the power module is impacted by increasing the switching frequency above a certain threshold, although its size is decreased by increasing the operating frequency. This is because the skin effect greatly increases with the frequency at which current flows through the conductor's surface. Similar to the skin effect, the proximity effect limits the passage of current to surfaces that are in close proximity to one another. Conductor size and layer count must be optimized for closeness in high-frequency systems. An increase in interleaving can be made with a planar transformer to lessen the proximity effect. The degree of leakage produced by this interleaving can be adjusted to help with power transmission and contribute to ZVS.

Planar transformers were employed in this reference design because they have the following benefits over conventional transformers:

• The power density in planar magnetics is extremely high. When compared to a traditional transformer with the same power rating, they are more space-efficient and compact.
• They have the capacity to increase interleaving to lower conductor losses in the AC system.
• They have predictable turns and layer spacing, which results in predictable parasites. It is possible to maintain very predictable and precise values for both the leakage inductance and the intra-winding capacitances.
• With planar magnetics, the leakage inductance may be tightly controlled.
• The utilization of a compact transformer allows for the integration of an additional shim inductor without the need for an independent component on the board. This section focuses on the specific planar transformer employed in this application and provides details regarding the associated loss figures. Leakage inductors by themselves are unable to guarantee gentle switching at light loads. As was previously demonstrated, raising the inductor value increases the RMS currents while expanding the soft switching range. In general, a leaking inductor is employed to enable soft switching, but its effectiveness is limited to loads that are approximately half or one-third of the rated load. To achieve soft switching at lighter loads, the magnetizing inductance of the transformer is utilized. For this optimization, the magnetizing inductance is typically set as a starting point at 10 times the value of the leakage inductance.

4.3.8 SiC MOSFET Selection

The selection of SiC switches was based on the following factors:

• The SiC MOSFET switches more quickly than a conventional Si device, which lowers switching losses.

• The SiC MOSFET for DAB applications has a substantially smaller reverse recovery charge, which lowers voltage and current overshoot.

• Conduction losses throughout the device's lifetime will be greatly reduced by a lower state resistance.

• The switches can block greater voltages without breaking down.

CREE

C3M0016120K

Silicon Carbide Power MOSFET
C3M™ MOSFET Technology

N-Channel Enhancement Mode

V_{DS}	1200 V
$I_{D\ @\ 25^{\circ}C}$	115 A
$R_{DS(on)}$	16 mΩ

Features

- 3rd generation SiC MOSFET technology
- Optimized package with separate driver source pin
- 8mm of creepage distance between drain and source
- High blocking voltage with low on-resistance
- High-speed switching with low capacitances
- Fast intrinsic diode with low reverse recovery (Q_{rr})
- Halogen free, RoHS compliant

Benefits

- Reduce switching losses and minimize gate ringing
- Higher system efficiency
- Reduce cooling requirements
- Increase power density
- Increase system switching frequency

Applications

- Solar inverters
- EV motor drive
- High voltage DC/DC converters
- Switched mode power supplies
- Load switch

Package

Halogen-Free

RoHS

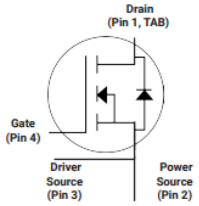

Part Number	Package	Marking
C3M0016120K	TO 247-4	C3M0016120K

Figure 4.4 Primary Side MOSFET switches Rating

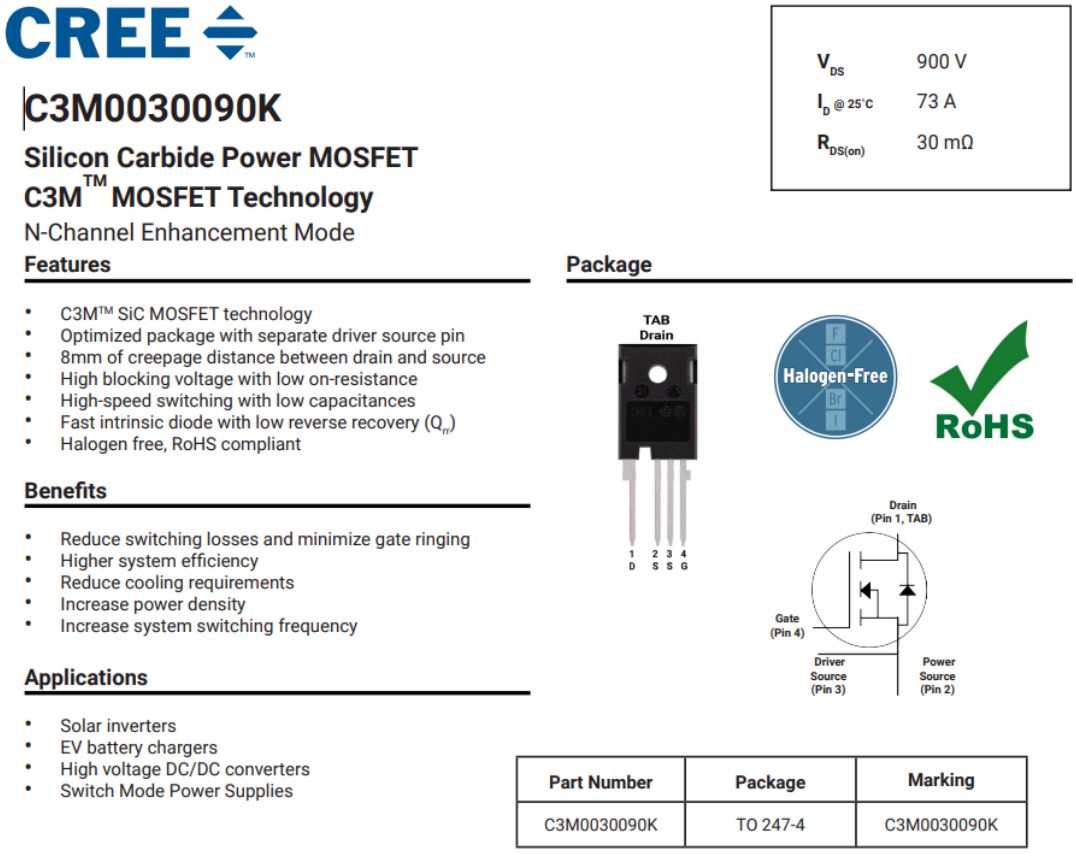

Figure 4.5 Secondary Side MOSFET switches rating

4.3.9 Loss Analysis

The theoretical efficiency figures derived from the dual-active bridge are reviewed in this section. To determine the losses in different components, the average and RMS currents flowing through both the primary and secondary sides are estimated. The scope of this design does not include information on how equations are actually derived. At a phase shift of 90°, a dual-active bridge experiences its maximum power transmission. But for power transfer, a significant phase shift necessitates a high leakage inductance. The efficiency of the converter is impacted by increased RMS currents on the primary and secondary sides caused by using a high inductor.

Table 4.1. Specification of DAB Converter

PARAMETERS	SPECIFICATIONS
DC-Input Voltage	800V
Input Current	12.5 A
Switching Frequency	100 kHZ

Turns Ratio	1:0.625
Leakage Inductance	35 µH
Output Capacitance	250 µF
Power Rating	10 kW
Output Voltage	500 V
Output Current	20 A

4.4 Closed loop control of DAB Converter

A rechargeable battery is continually charged at a constant current using constant current charging to prevent overcurrent charge issues. This constant-current technique can be used to charge both lithium-ion and lead-acid batteries. This closed-loop control implements the logic for the phase shift offered to the secondary side switches of the DAB converter. The reference-rated current and battery current are compared, and the difference in error is sent to the PI controller. Gains in PI can be managed in a variety of ways. The Ziegler and Nicholas method, which is often employed for PI tuning, is one of them.

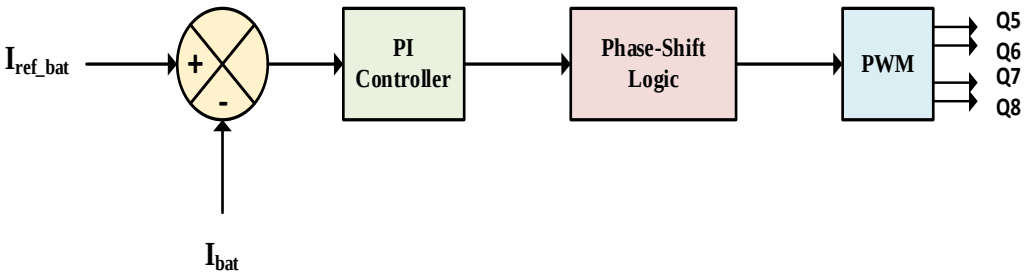

Figure 4.6 Block Diagram of Control Strategy

Table 4. 2.PI Controller Values

PARAMETERS	VALUES
k_p	0.005
k_i	2.3

The output of the PI controller, as shown in Fig. 7, is transmitted through a PWM block and a phase-shift logic block to produce a phase shift between the transformer voltages on both sides of the converter.

4.5 Simulation Results

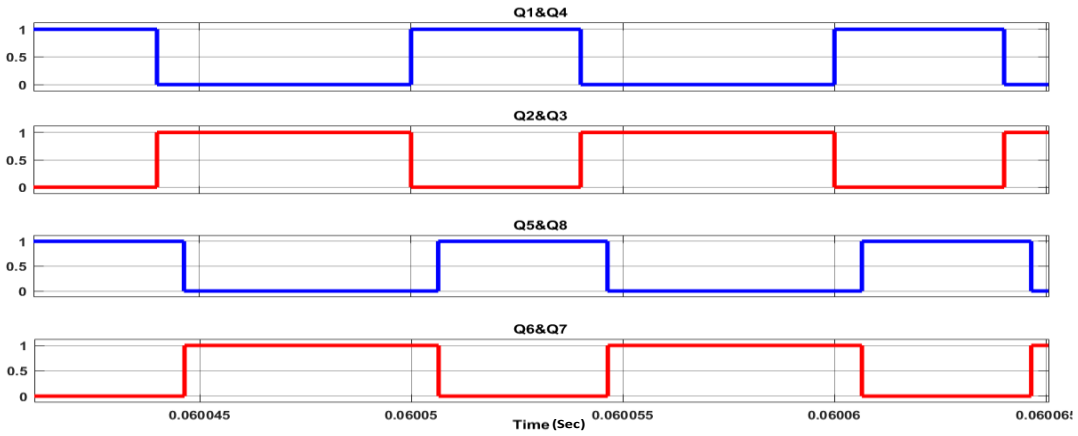

Figure 4.7 Switching sequence for Primary and Secondary Side Switches

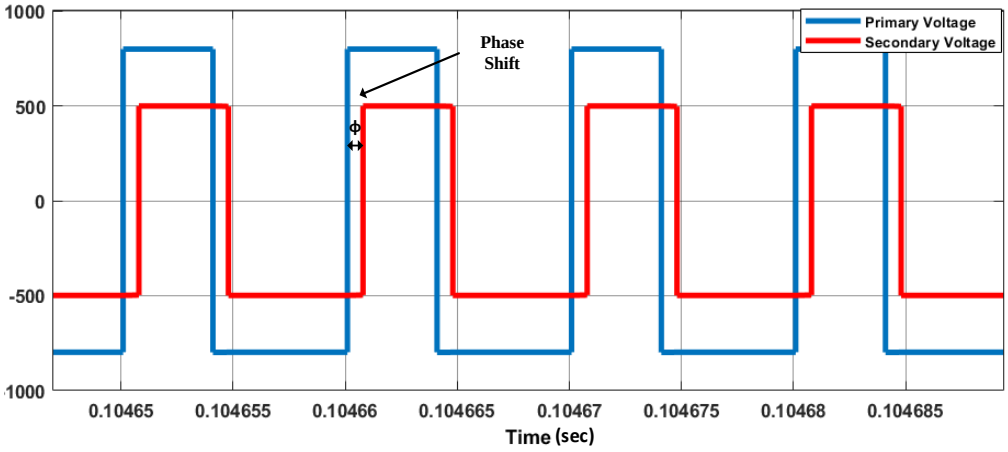

Figure 4.8 Phase Shift between Primary and Secondary

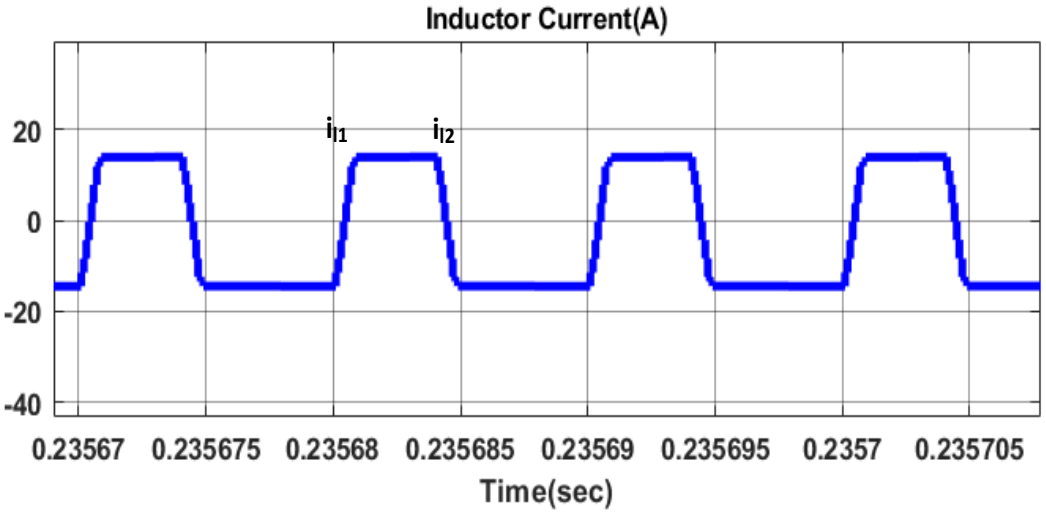

Figure 4.9 Inductor Current

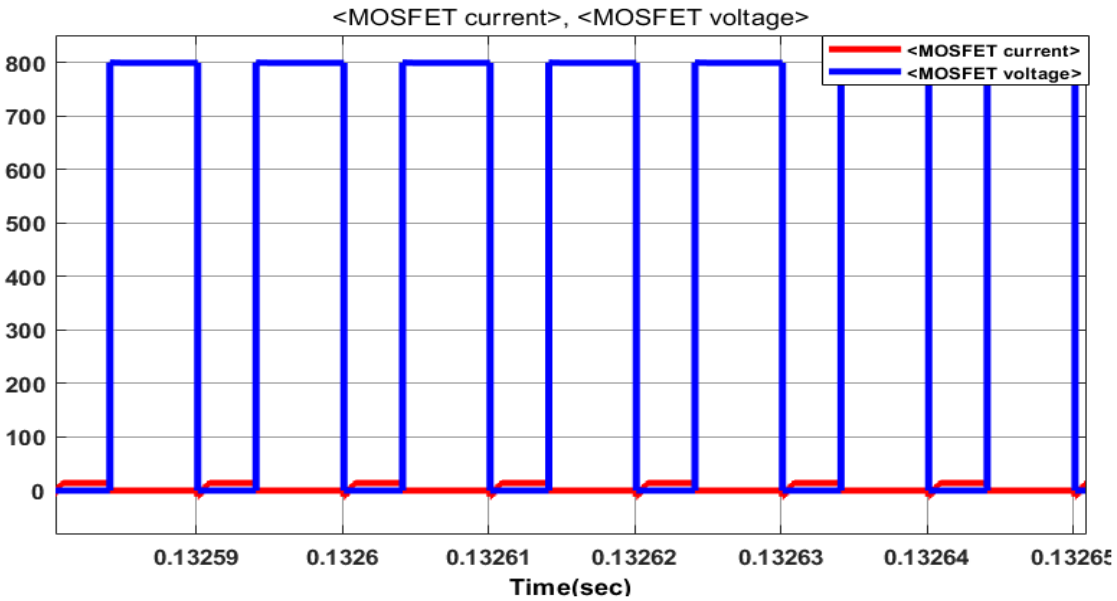

Figure 4.10 ZVS in Primary Side H-Bridge of DAB Converter

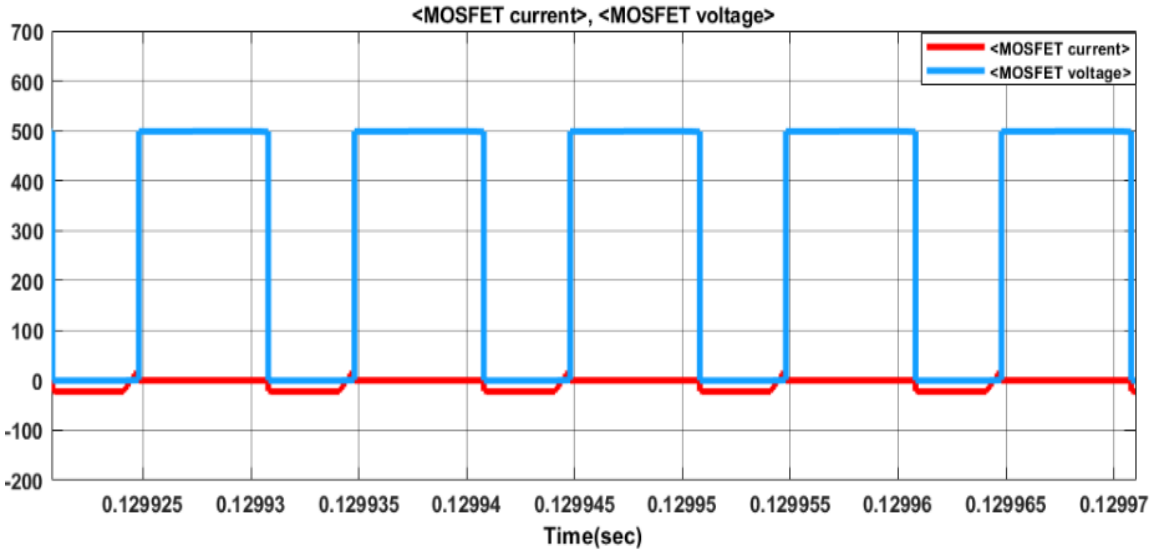

Figure 4.11 ZVS in Secondary Side H-Bridge of DAB Converter

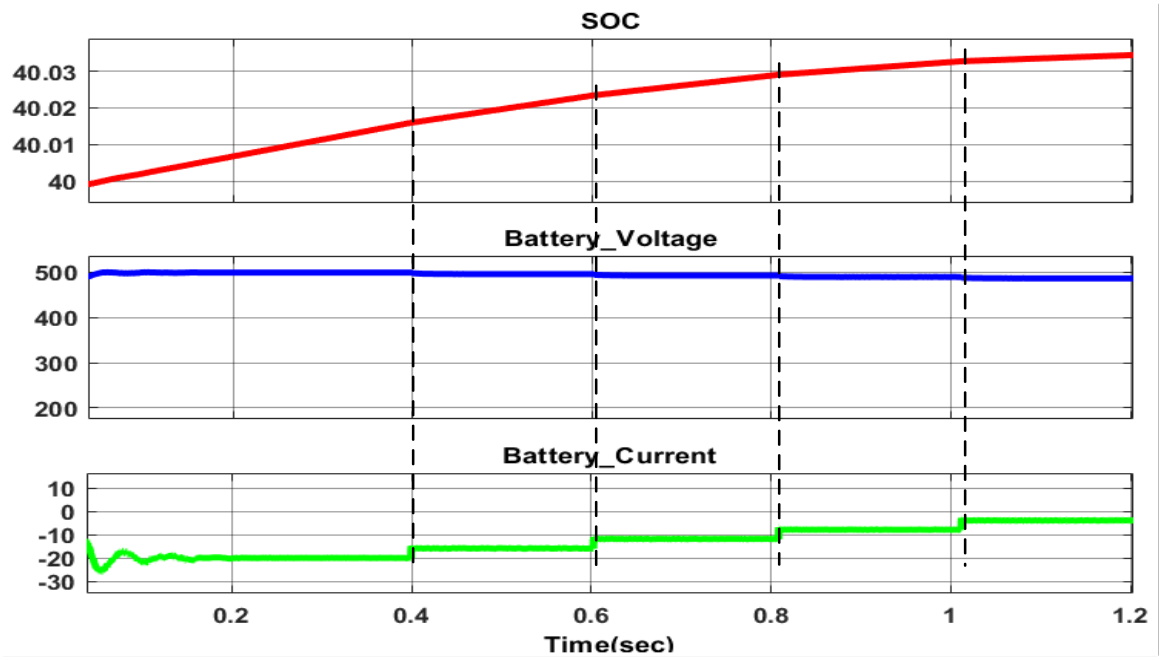

Figure 4.12 Battery SOC, Voltage and Current for different Load Variation

4.6 Conclusion

Incorporating an LC filter at its output, the DAB converter's construction and control are discussed in this chapter for use in battery charging applications. Battery charging with a variable load is intended for the current control technique. The switching pattern for primary and secondary side bridge switches is depicted in Fig. 4.5. Figures 4.6 and 4.7 demonstrate the phase shift between voltages and the current through the leaking inductor, respectively, for the power transmission. In Figs. 4.8 and 4.9, the ZVS obtained for the primary and secondary side switches under various loading conditions is depicted. Therefore, ZVS can be accomplished by selecting the appropriate leakage inductance and snubber capacitance linked in parallel to MOSFETs. The battery charging process is shown in Fig. 4.10, along with the impact of load changes on SOC, battery voltage, and battery current.

Up to time t = 0.4 s, there is no load connected in parallel with the battery. The battery's SOC is rapidly increasing as a result. At time t = 0.4, a load is switched in parallel with the battery. Even though at this time the growth in SOC rate somehow slows down and the current passing through the battery also decreases, the controller is designed in such a way that it tries to maintain the rated value of battery voltage. An equal amount of time is spent between each of the three extra loads that are connected in parallel. At time t = 1.02, when all loads are connected, SOC almost goes flat and scarcely increases.

The closed-loop results indicate that the existing controller performs satisfactorily. Additionally, it has been confirmed that adding an LC filter at the output preserves the proper output voltage and lessens battery current ripple. The charging procedure is then carried out under four parallel load variations. The total findings demonstrate the battery bank's good voltage and current response to changing loads.

CHAPTER-5
CONCLUSION AND FUTURE SCOPE

This endeavor focuses on the development of electric vehicle (EV) charger controllers, with particular emphasis on the two crucial conversion stages: AC-DC (first) and DC-DC (second). These converters play a vital role in the EV charger as they enable the charging and discharging of the battery pack while also addressing reactive power compensation. Both converters are intended to work in both directions for this reason. MOSFET switches with an anti-parallel diode are used to create the converters. The EV charger can both charge the battery pack and transmit battery power to the grid or a local load.

An EV charger controller handles the management of active/reactive power, grid-side current, DC link voltage, and battery current within the charging system. The proposed system regulates three quantities: active/reactive power, grid side current, and AC-DC converter control. The remaining two values, The DC-DC converter assumes control over the DC link voltage and battery current. In this situation, three references are furnished, while the remaining two references are generated by the converter itself.

The control of an AC-DC converter is done using decoupled dq control with DC voltage sensing. This control keeps the Grid voltage and Grid current in same phase along with that it also maintains the output voltage.

The control of DC-DC converter is done using Constant current control technique under variable load condition. The controller generates the desired phase shift between the primary and secondary bridge according to load variation. The ripple from output current is reduce using inductor as a filter at the output.

The future scope for grid-tied active front-end rectifier-fed dual-active-bridge converter in EV battery charging is highly promising. With its bidirectional power flow capability, efficient power transfer, advanced control features, scalability, and the ongoing advancements in power semiconductor devices. For further improvement, renewable energy sources such as solar and wind power with advanced energy management systems can be utilized to ensure charging of EV batteries during source

availability. It offers a robust and versatile solution for fast, reliable, and environmentally friendly EV charging infrastructure, contributing to the transition towards a greener and more energy-efficient future.

REFERENCES

[1] B. Nykvist and M. Nilsson, “Rapidly falling costs of battery packs for electric vehicles,” Nature climate change, vol. 5, no. 4, p. 329, 2015.

[2] S. Manzetti and F. Mariasiu, “Electric vehicle battery technologies: From present state to future systems,” Renewable and Sustainable Energy Reviews, vol. 51, pp. 1004–1012, 2015.

[3] S. Ahmed et al., “Enabling fast charging–a battery technology gap assessment,” Journal of Power Sources, vol. 367, pp. 250–262, 2017.

[4] M. Keyser et al., “Enabling fast charging–battery thermal considerations,” Journal of Power Sources, vol. 367, pp. 228–236, 2017.

[5] “Sae electric vehicle and plug in hybrid electric vehicle conductive charge coupler,” SAE J1772, pp. 1–1, October 2017.

[6] A. Burnham et al., “Enabling fast charging–infrastructure and economic considerations,” Journal of Power Sources, vol. 367, pp. 237– 249, 2017.

[7] H. Feng, T. Cai, S. Duan, J. Zhao, X. Zhang, and C. Chen, “An lcc-compensated resonant converter optimized for robust reaction to large coupling variation in dynamic wireless power transfer,” IEEE Transactions on Industrial Electronics, vol. 63, no. 10, pp. 6591–6601, Oct 2016.

[8] F. Musavi and W. Eberle, “Overview of wireless power transfer technologies for electric vehicle battery charging,” IET Power Electronics, vol. 7, no. 1, pp. 60–66, January 2014 .

[9] D. Patil, M. K. McDonough, J. M. Miller, B. Fahimi, and P. T. Balsara, “Wireless power transfer for vehicular applications: Overview and challenges,” IEEE Transactions on Transportation Electrification, vol. 4, no. 1, pp. 3–37, March 2018 .

[10] M. Smith and J. Castellano, “Costs associated with non-residential electric vehicle supply equipment: Factors to consider in the implementation of electric vehicle charging stations,” New West Technologies, LLC, Tech. Rep., 2015.

[11] Q. Wu, A. H. Nielsen, J. Østergaard, S. T. Cha, and Y. Ding, “Impact study of electric vehicle (ev) integration on medium voltage (mv) grids,” in 2011 2nd IEEE PES International Conference and Exhibition on Innovative Smart Grid Technologies. IEEE, 2011, pp. 1–7.

[12] K. Clement-Nyns, E. Haesen, and J. Driesen, “The impact of charging plug-in hybrid electric vehicles on a residential distribution grid,” IEEE Transactions on Power Systems, vol. 25, no. 1, pp. 371–380, Feb 2010.

[13] M. J. Rutherford and V. Yousefzadeh, “The impact of electric vehicle battery charging on distribution transformers,” in 2011 Twenty-Sixth Annual IEEE Applied Power Electronics Conference and Exposition (APEC), March 2011, pp. 396–400.

[14] H. Shareef, M. M. Islam, and A. Mohamed, “A review of the stage-of the-art charging technologies, placement methodologies, and impacts of electric vehicles,” Renewable and Sustainable Energy Reviews, vol. 64, pp. 403–420, 2016.

[15] C. Capasso and O. Veneri, “Experimental study of a dc charging station for full electric and plug in hybrid vehicles,” Applied energy, vol. 152, pp. 131–142, 2015.

[16] D. Sbordone, I. Bertini, B. Di Pietra, M. C. Falvo, A. Genovese, and L. Martirano, “Ev fast charging stations and energy storage technologies: A real implementation in the smart micro grid paradigm,” Electric Power Systems Research, vol. 120, pp. 96–108, 2015.

[17] S. Bai, D. Yu, and S. Lukic, “Optimum design of an ev/phev charging station with dc bus and storage system,” in 2010 IEEE Energy Conversion Congress and Exposition, Sep. 2010, pp. 1178–1184.

[18] J. C. Mukherjee and A. Gupta, “A review of charge scheduling of electric vehicles in smart grid,” IEEE Systems Journal, vol. 9, no. 4, pp. 1541–1553, Dec 2015.
[19] S. Rajakaruna, F. Shahnia, and A. Ghosh, Plug in electric vehicles in smart grids: charging strategies. Springer, 2014.
[20] Z. Xu, Z. Hu, Y. Song, Z. Luo, K. Zhan, and J. Wu, “Coordinated charging strategy for pevs charging stations,” in 2012 IEEE Power and Energy Society General Meeting, July 2012, pp. 1–8.
[21] M. Tabari and A. Yazdani, “An energy management strategy for a dc distribution system for power system integration of plug-in electric vehicles,” IEEE Transactions on Smart Grid, vol. 7, no. 2, pp. 659–668, March 2016.
[22] S. Negarestani, M. Fotuhi-Firuzabad, M. Rastegar, and A. RajabiGhahnavieh, “Optimal sizing of storage system in a fast charging station for plug-in hybrid electric vehicles,” IEEE Transactions on Transportation Electrification, vol. 2, no. 4, pp. 443–453, Dec 2016.
[23] P. You, Z. Yang, M. Chow, and Y. Sun, “Optimal cooperative charging strategy for a smart charging station of electric vehicles,” IEEE Transactions on Power Systems, vol. 31, no. 4, pp. 2946–2956, July 2016.
[24] S. Y. Derakhshandeh, A. S. Masoum, S. Deilami, M. A. S. Masoum, and M. E. Hamedani Golshan, “Coordination of generation scheduling with pevs charging in industrial microgrids,” IEEE Transactions on Power Systems, vol. 28, no. 3, pp. 3451–3461, Aug 2013.
[25] F. Koyanagi and Y. Uriu, “A strategy of load leveling by charging and discharging time control of electric vehicles,” IEEE Transactions on Power Systems, vol. 13, no. 3, pp. 1179–1184, Aug 1998.
[26] C. D. White and K. M. Zhang, “Using vehicle-to-grid technology for frequency regulation and peak-load reduction,” Journal of Power Sources, vol. 196, no. 8, pp. 3972–3980, 2011.
[27] T. Wu, Q. Yang, Z. Bao, and W. Yan, “Coordinated energy dispatching in microgrid with wind power generation and plug-in electric vehicles,” IEEE Transactions on Smart Grid, vol. 4, no. 3, pp. 1453–1463, Sep. 2013.
[28] M. Kesler, M. C. Kisacikoglu, and L. M. Tolbert, “Vehicle-to-grid reactive power operation using plug-in electric vehicle bidirectional offboard charger,” IEEE Transactions on Industrial Electronics, vol. 61, no. 12, pp. 6778–6784, Dec 2014.
[29] J. Y. Yong, V. K. Ramachandaramurthy, K. M. Tan, and N. Mithulananthan, “Bi-directional electric vehicle fast charging station with novel reactive power compensation for voltage regulation,” International Journal of Electrical Power & Energy Systems, vol. 64, pp. 300–310, 2015.
[30] W. Hu, C. Su, Z. Chen, and B. Bak-Jensen, “Optimal operation of plug-in electric vehicles in power systems with high wind power penetrations,” IEEE Transactions on Sustainable Energy, vol. 4, no. 3, pp. 577–585, July 2013.
[31] M. Ghofrani, A. Arabali, M. Etezadi-Amoli, and M. S. Fadali, “Smart scheduling and cost-benefit analysis of grid-enabled electric vehicles for wind power integration,” IEEE Transactions on Smart Grid, vol. 5, no. 5, pp. 2306–2313, Sep. 2014.
[32] Y. Cao, N. Wang, G. Kamel, and Y. Kim, “An electric vehicle charging management scheme based on publish/subscribe communication framework,” IEEE Systems Journal, vol. 11, no. 3, pp. 1822–1835, Sep. 2017.
[33] Y. Cao, Y. Miao, G. Min, T. Wang, Z. Zhao, and H. Song, “Vehicular-publish/subscribe (v-p/s) communication enabled on-the move ev charging management,” IEEE Communications Magazine, vol. 54, no. 12, pp. 84–92, December 2016.

[34] I. S. Bayram, G. Michailidis, M. Devetsikiotis, and F. Granelli, "Electric power allocation in a network of fast charging stations," IEEE Journal on Selected Areas in Communications, vol. 31, no. 7, pp. 1235– 1246, July 2013.
[35] X. Dong, Y. Mu, H. Jia, J. Wu, and X. Yu, "Planning of fast ev charging stations on a round freeway," IEEE Transactions on sustainable Energy, vol. 7, no. 4, pp. 1452–1461, 2016.
[36] A. Khaligh and S. Dusmez, "Comprehensive topological analysis of conductive and inductive charging solutions for plug-in electric vehicles," IEEE Transactions on Vehicular Technology, vol. 61, no. 8, pp. 3475–3489, Oct 2012.
[37] M. Yilmaz and P. T. Krein, "Review of battery charger topologies, charging power levels, and infrastructure for plug-in electric and hybrid vehicles," IEEE Transactions on Power Electronics, vol. 28, no. 5, pp. 2151–2169, May 2013.
[38] H. van Hoek, M. Neubert, and R. W. De Doncker, "Enhanced modulation strategy for a three-phase dual active bridge-boosting efficiency of an electric vehicle converter," IEEE Transactions on Power Electronics, vol. 28, no. 12, pp. 5499–5507, Dec 2013.
[39] L. Xue, Z. Shen, D. Boroyevich, P. Mattavelli, and D. Diaz, "Dual active bridge-based battery charger for plug-in hybrid electric vehicle with charging current containing low frequency ripple," IEEE Transactions on Power Electronics, vol. 30, no. 12, pp. 7299–7307, Dec 2015.
[40] L. Xue, M. Mu, D. Boroyevich, and P. Mattavelli, "The optimal design of gan-based dual active bridge for bi-directional plug-in hybrid electric vehicle (phev) charger," in 2015 IEEE Applied Power Electronics Conference and Exposition (APEC), March 2015, pp. 602–608.
[41] R. W. De Doncker, D. M. Divan, and M. H. Kheraluwala, "A threephase soft-switched high power density dc/dc converter for high power applications," in Conference Record of the 1988 IEEE Industry Applications Society Annual Meeting, Oct 1988, pp. 796–805 vol.1.
[42] H. Akagi, T. Yamagishi, N. M. L. Tan, S. Kinouchi, Y. Miyazaki, and M. Koyama, "Power-loss breakdown of a 750-v 100-kw 20- khz bidirectional isolated dc-dc converter using sic-mosfet/sbd dual modules," IEEE Transactions on Industry Applications, vol. 51, no. 1, pp. 420–428, Jan 2015.
[43] J. E. Huber and J. W. Kolar, "Applicability of solid-state transformers in today's and future distribution grids," IEEE Transactions on Smart Grid, vol. 10, no. 1, pp. 317–326, Jan 2019.
[44] N. M. L. Tan, T. Abe, and H. Akagi, "Design and performance of a bidirectional isolated dc-dc converter for a battery energy storage system," IEEE Transactions on Power Electronics, vol. 27, no. 3, pp. 1237–1248, March 2012.
[45] H. Wen, W. Xiao, and B. Su, "Nonactive power loss minimization in a bidirectional isolated dc-dc converter for distributed power systems," IEEE Transactions on Industrial Electronics, vol. 61, no. 12, pp. 6822– 6831, Dec 2014.
[46] A. Rodríguez, A. Vázquez, D. G. Lamar, M. M. Hernando, and J. Sebastián, "Different purpose design strategies and techniques to improve the performance of a dual active bridge with phase-shift control," IEEE Transactions on Power Electronics, vol. 30, no. 2, pp. 790–804, Feb 2015.
[47] B. Zhao, Q. Song, W. Liu, and W. Sun, "Current-stress-optimized switching strategy of isolated bidirectional dc-dc converter with dual phase-shift control," IEEE Transactions on Industrial Electronics, vol. 60, no. 10, pp. 4458–4467, Oct 2013.

[48] C. Cecati, A. Dell'Aquila, A. Lecci, and M. Liserre, "Implementation issues of a fuzzy-logic-based three-phase active rectifier employing only voltage sensors," IEEE

Trans. Ind. Electron., vol. 52, no. 2, pp. 378–385, Apr. 2005.
[49] T. Thien, D. Schweer, D. vom Stein, A. Moser, and D. U. Sauer, “Realworld operating strategy and sensitivity analysis of frequency containment reserve provision with battery energy storage systems in the german market,” J. Energy Storage, vol. 13, pp. 143–163, Oct. 2017.
[50] M. Y. Metwly, M. S. Abdel-Majeed, A. S. Abdel-Khalik, R. A. Hamdy, M. S. Hamad, and S. Ahmed, “A review of integrated on-board EV battery chargers: Advanced topologies, recent developments and optimal selection of FSCW slot/pole combination,” IEEE Access, vol. 8, pp. 85216–85242, May 2020.
[51] N. Hou, P. Gunawardena, X. Wu, L. Ding, Y. Zhang, and Y. W. Li, ‘‘An input-oriented power sharing control scheme with fast-dynamic response for ISOP DAB DC–DC converter,’’ IEEE Trans. Power Electron., vol. 37, no. 6, pp. 6501–6510, Jun. 2022.
[52] T. Zhao, G. Wang, S. Bhattacharya, and A. Q. Huang, “Voltage and power balance control for a cascaded h-bridge converter-based solid-state transformer,” IEEE Transactions on Power Electronics, vol. 28, no. 4, pp. 1523–1532, 2013.
[53] A. Khaligh and M. D'Antonio, “Global Trends in High-Power On-Board Chargers for Electric Vehicles,” IEEE Trans. on Vehi. Tech., vol. 68, no. 4, pp. 3306-3324, April 2019.
[54] L.-R. Chen, S.-L. Wu, D.-T. Shieh, and T.-R. Chen, "Sinusoidal ripple current charging strategy and optimal charging frequency for Li-ion batteries," IEEE Trans. Ind. Electron., vol. 60, no. 1, pp. 88-97, 2013.
[55] B. Hua, C. C. Mi, and S. Gargies, The Short-Time-Scale Transient Processes in High-Voltage and High-Power Isolated Bidirectional DC-DC Converters, IEEE Transactions on Power Electronics, vol. 23, no. 6, pp. 2648-2656, 2008.
[56] T. Tanaka, T. Sekiya, H. Tanaka, M. Okamoto and E. Hiraki, “Smart Charger for Electric Vehicles with Power-Quality Compensator on Single-Phase Three-Wire Distribution Feeders,” IEEE Trans. on Indus. Appl., vol. 49, no. 6, pp. 2628-2635, Nov.-Dec. 2013.
[57] C. Jin, P. Wang, J. Xiao, Y. Tang, and F. H. Choo, “Implementation of hierarchical control in DC microgrids,” IEEE transactions on industrial electronics, vol. 61, no. 8, pp.4032-4042, Aug. 2014.
[58] Y. Yan, H. Bai, A. Foote and W. Wang, "Securing Full-Power-Range Zero-Voltage Switching in Both Steady-State and Transient Operations for a Dual-Active-Bridge-Based Bidirectional Electric Vehicle Charger," in IEEE Transactions on Power Electronics, vol. 35, no. 7, pp. 7506-7519, July 2020, doi: 10.1109/TPEL.2019.2955896.
[59] Z. Zhang, Y. Xiao, M. A. E. Andersen and K. Sun, "Impact on ZVS Operation by Splitting Inductance to Both Sides of Transformer for 1- MHz GaN Based DAB Converter," in IEEE Transactions on Power Electronics, doi: 10.1109/TPEL.2020.2988638.
[60] A. Khaligh and S. Dusmez, "Comprehensive Topological Analysis of Conductive and Inductive Charging Solutions for Plug-In Electric Vehicles," in IEEE Transactions on Vehicular Technology, vol. 61, no. 8, pp. 3475-3489, Oct. 2012.
[61] V. M. Iyer, S. Gulur, G. Gohil and S. Bhattacharya, "Extreme fast charging station architecture for electric vehicles with partial power processing," 2018 IEEE Applied Power Electronics Conference and Exposition (APEC), San Antonio, TX, 2018, pp. 659-665.

[62] N. Tuan, W. Jehyuk, and N. Kwanghee, "A single-phase bidirectional dual active half-bridge converter," in Applied Power Electronics Conference and Exposition (APEC), 2012 Twenty-Seventh Annual IEEE, 2012, pp. 1127-1133.

[63] M. Uno and K. Tanaka, “Influence of high-frequency charge-discharge cycling induced by cell voltage equalizers on the life performance of lithium-ion cells,” Vehicular Technology, IEEE Transactions on, vol. 60, pp. 1505–1515, 2011.

LIST OF PUBLICATIONS

[1]. Ashish Mishra, Mukhtiar Singh "A 10-kW Active Front End Rectifier Fed Dual Active Bridge Converter for EV Charging", IEEE 4 th International Conference of Emerging Technology 2023, Belagavi, India (26-28 May 2023) **(Presented)**

Jain College of Engineering
Belagavi, India

IEEE BANGALORE SECTION

4th International Conference of Emerging Technology
(INCET 2023)

26th – 28th May 2023

Certificate

This is to certify that Dr./Prof./Mr./Ms. ***Ashish Mishra*** *has presented paper entitled* ***A 10-kW Active Front End Rectifier Fed Dual Active Bridge Converter For EV Charging*** *in 4th International Conference of Emerging Technology (INCET 2023) during 26th to 28th May 2023.*

Dr. Krupa Rasane
Convener - INCET 2023

Dr. J. Shivakumar
General Chair - INCET 2023